Mapping past, present and future dew and rain water resources for biocrust evolution in southern Africa

Marc Muselli, Daniel Beysens

Mapping past, present and future dew and rain water resources for biocrust evolution in southern Africa

M. Muselli[1,2] and D. Beysens[2,3]

[1] Università di Corsica Pasquale Paoli, Avenue du 9 septembre, BP 52, 20250 Corte, France

[2] OPUR, 2 rue Verderet, 75016 Paris, France

[3] Physique et Mécanique des Milieux Hétérogènes, CNRS, ESPCI Paris - PSL University, Sorbonne Université, Sorbonne Paris Cité, 10 rue Vauquelin, 75005 Paris, France

Corresponding author: Daniel Beysens, ph: +33(0)689864717, daniel.beysens@espci.fr

Abstract

Biocrust sustainability relies on dew and rain availability. A study of dew and rain resources in amplitude and frequency and their evolution is presented from year 2001 to 2020 in southern Africa (Namibia, Botswana, South Africa) where many biocrust sites have been identified. The evaluation of dew is made from a classical energy balance model using meteorological data collected in 18 stations, where are also collected rain data. One observes a strong correlation between the frequency of dew and rain and the corresponding amplitudes. There is a general tendency to see a decrease in dew yield and dew frequency with increasing distance from the oceans, located west, east and south, due to decreasing RH, with a relative minimum in the desert of Kalahari (Namibia). Rain amplitude and frequency decreases when

going to west and north. Short-term dew/rain correlation shows that largest dew yields clearly occur during about three days after rainfall, particularly in the sites where humidity is less.

The evolution in the period corresponds to a decrease of rain precipitations and frequency, chiefly after 2010, an effect which has been cyclic since now. The effect is more noticeable towards north. An increase of dew yield and frequency is observed, mainly in north and south-east. It results in an increase of the dew contribution with respect to rain, especially after 2010. As no drastic changes in the distribution of biomass of biocrusts have been reported in this period, it is likely that dew should compensate for the decrease in rain precipitation. Since the growth of biocrust is related to dew and rain amplitude and frequency, future evolution should be characterized by either the rain cycle or, due to global change, an acceleration of the present tendency, with more dew and less rainfalls.

Keywords

Biocrust; dew and rain evolution; dew/rain ratio; dew/rain correlation; southern Africa; climate change

1. Introduction

Biocrust are typically found in drylands with arid or semi-arid ecosystems. In great interaction with the soil, biocrust concern cyanobacteria, lichens, algae and mosses. These organisms contribute strongly in the ecosystem’s functioning and plant organization and are present all around the world.

Numerous works detail their physical, chemical and biological characteristics in semi-arid or arid climates. Negev (Jacobs et al., 2002; Kidron and Tal, 2012), Europe (Raggio et al., 2021),

Spain (Cano-Díaz et al., 2018), China (Yao et al., 2019), USA (Aguirre-Gutiérrez et al., 2019) are a few examples. According to Chen et al. (2020), biocrust correspond to 30% of global drylands. It is in China, Australia, North America and Spain in Europe that are found the more studied biocrust sites. In the present study, a representative area for biocrust studies was chosen in a less investigated area, the southern part of Africa. Namibia, South Africa and Bostwana are the main countries involved in this study, representing 18 sites of measurement (7 in Namibia, 7 in South Africa and 4 in Bostwana, respectively). One should note that, these locations are based on previous works of a few scholars within certain research sites and cannot obviously replace an objective map. A map of soil can help to locate biocrust, it is given in Fig. 1 together with the above studied sites.

Moisture from atmosphere (rainfall, fog, dew, vapor absorption) plays an important role in sustaining life in arid or semi-arid climates. Pan et al. (2010) concluded on the mutual enhanced effect between dew and artificially revegetation ecosystems in the arid desert ecosystem in Shapotou (China). Li et al. (2021a,b), in a recent paper, determine that biocrust benefits from non-rainfall water deposition and modify their distribution in drylands soils. Dewfall can be presented as a critical source of water in deserts environments allowing to determine the sustainability of sand to stabilize planted vegetation (Zhuang and Zhao, 2017). Dew, fog and rain can play an important role for the development of biocrust in semi-arid regions. Kidron (2020) suspects dew to be a necessary water source for cyanobacteria. Biocrust alter non-rainfall distribution by depth, concentrating it in the surface (Li et al., 2021a, b). Biocrust can boost the use of non-rainfall water according to Ouyang et al. (2017). Büdel et al. (2009) conclude their study by noting that the time frequency of rain precipitations is more important than their amount.

The amount and frequency of rain and dew are then the main factors which influence the growth of biocrust. This paper aims to evaluate the evolution of these contributions to over a

long period of time (20 years, from 2001 to 2020) in order to put in evidence the long term trend and extrapolate to the near future. Because certain data are lacking before 2011, a few analyses are restricted to 10 years (2011-2020). The paper is organized as follows. After having reported on measurements and methods in Section 2, mainly concerning the physical model used to determine the dew yields, Section 3 is devoted to the main results with maps i) for dew and rain atmospheric deposition, ii) cumulative rainfall and dew yields comparisons and iii) short time and longtime evolution of dew and rainfalls yield and frequency. A Section 4 is devoted to discussions and relation of the rain and dew studies with biocrust.

2. Meteorological data and methods

2.1. Dew yield estimation from meteorological data

In order to estimate the dew potential, Beysens (2016) developed an energy balance model which, thanks to some approximation, uses only a few classical meteorological data without adjustable parameters: cloud cover (N, oktas), wind speed (V, m.s^{-1}), air temperature (T_a, °C), air relative humidity (RH, %) and dew point temperature (T_d, °C). Near the ground level where dew forms, in the atmospheric boundary layer, the contribution from water vapor (about 0.2–2% by volume) and, to a lower extent, carbon dioxide (about 0.03% in volume) is of great importance for the radiative balance, with radiation from water vapor being by far the more important of the two. The results are concerned with dew yields h [mm. $(\Delta t)^{-1}$] where Δt corresponds to the period (in h.) of the analyzed data. It is assumed that the substrate emissivity is unity (which is close to the emissivity ≈ 0.98 of a wet substrate, see Trosseille et al., 2021) and is thermally insulated from below. The data can be obtained from the airport meteo stations by using the following formulation:

$$h = \left(\frac{\Delta t}{12}\right)(HL + RE) \quad (1)$$

The factor Δt is the measurement period of the data (here 6, 3 or 1 h. depending on the stations). The data for $h > 0$ correspond to condensation and $h < 0$ to evaporation, which have to be discarded. The quantity *HL* represents the convective heat losses between air and condenser, with a cut-off for windspeed $V > V_0 = 4.4$ m.s^{-1} where condensation vanishes:

$$h = \begin{cases} \left(\frac{\Delta t}{12}\right)[0.06(T_d - T_a) + RE] & \text{if } V < V_0 \\ 0 & \text{if } V > V_0 \end{cases} \quad (2)$$

The quantity RE is the available radiative energy, which depends on air water content (measured by the dew point temperature T_d, in °C), site elevation *H* (in km) and cloud cover *N* (in oktas):

$$RE = 0.37 \times (1 + 0.204323H - 0.0238893H^2 - (18.0132 - 1.04963H + 0.21891H^2) \times 10^{-3}T_d)\left(\frac{T_d+273.15}{285}\right)^4 (1 - \frac{\mathrm{N}}{8}) \quad (3)$$

By filtering the rain and fog events and integrating the time series on a daily time-step corresponding to $h > 0$, calculated daily yields and their cumulated values are obtained. We give an example of calculation in Appendix 1.

2.2. Studied area

The study area (Fig. 1) is characterized by a spatial extent of about 3 000 000 km^2 between 15° to 35° south latitude and 13° to 30° for east longitude. In the following are detailed the different climate characteristics of the countries.

Namibia (824 292 km² surface area). The country shows three different climates, the most prevalent being semi-arid (Köppen-Geiger classification BSh) and hot desert (BWh). The less frequent is cold desert climates (BWk). The climate is characterized by great differences in day and nighttime temperatures, low rainfall and overall low humidity. Along the coast, the average annual precipitation does not exceed 15 mm. Inside the country, the continental plateau has a more contrasted situation with abundant precipitations (> 500 mm). The dry season, between May to October, correspond to little or no rainfall during July and August. Wildlife uses mainly waterholes and rivers when the water sources dry up. In desert areas, the average minimum temperature is cold and can fall below freezing at night. The wet season, between November to April, present daytime temperatures of about 30°C with the first rains observed in November (mean rainfall 26 mm to a maximum in January with 91 mm). Sometimes, torrential downpours are observed in the afternoon up to March and April, where rainfall decrease and stops before the dry season.

Botswana (581 730 km² surface area). The climate is characterized as hot semi-arid, the dominant climate (Köppen-Geiger classification BSh), and hot desert (BWh). During summer months (November-March), a rainy season is observed with high temperatures. The mean annual rainfall varies from over 650 mm in the extreme northeast area (Chobe District) to a minimum of 250 mm in the extreme southwest part (Kgalagadi District). The winter season during May to August corresponds to the dry season with less than 10% of the annual rainfall. The variability of rainfall increases while the quantity decreases toward the south and west.

South Africa (1,22 million km² surface area). The country corresponds to a subtropical area, influenced by the vicinity of the oceans along the coastlines and the altitude of interior plateau (1 500 m in the dolerite-capped Roggeveld scarp in the south-west, to a height of 3 482 m in the KwaZulu-Natal Drakensberg). The country has several climatic zones depending on its geography: in the northwest, near the Atlantic coast stretching to the center of the country, the climate is mainly characterized by arid lime (BWh) or cold (BWk) deserts. In the south-east, the country offers a temperate climate with dry and hot (Csa) or warm (Csb) summers. Finally, along the southern coast of the country, we find a hot (BSh) or cold (BSk) arid climate with steppes but also a temperate zone, along the ocean between the towns of George and Port Elisabeth with dry winters and hot summers (Cwa). The eastern part of the country, which is more mountainous, is characterized by a predominantly temperate climate, without a dry season, with hot to temperate (Cfb) or cold (Cfc) summers. Mean rainfall is about 460 mm with a large dispersion according to the location. Usually, the western Cape presents major rainfalls in winter whereas the rest of the country exhibits summer rainfalls.

Figure 1

The spatial distribution of rainfall between Namibia, Bostwana and South Africa presents some differences in space and time (New et al., 2000). In Namibia, for the locations of Dante Cave at the north of the country, summer rainfall is observed from October to April, with mean annual rainfall between 500 and 600 $mm.yr^{-1}$, a value much less than the potential evapotranspiration estimated to 2900 $mm.yr^{-1}$ (Railsback and al., 2019). A similar behavior is observed at the frontier between Bostwana and South Africa (27°S, 21°E), with summer rainfall. The situation is more complex in South Africa. According to the location, one observes winter rainfall as in Cape Town with precipitations mainly during April to

September, weak precipitations but year-round in George and summer rainfall with a dry winter in Pretoria (Railsback and al., 2019).

2.3. Extraction data

All ground stations are installed on international or national airports where standard meteorological parameters are measured. The meteorological stations meet the data measurement standards of the World Meteorological Organization. Air T_a (°C) and dew T_d (°C) temperatures, relative humidity (*RH*, %), atmospheric pressure (*P*, Pa) are measured in a meteorological shelter, 1.5 m from the ground. The windspeed (*V*, km.h^{-1}) and direction (sectors or degrees) are measured at 10 m from the ground. Note that wind speed can be extrapolated at any height *z* above the ground by the classical logarithmic variation (see e.g. Pal Arya, 1988) $V(z) = V_{10}\ln\left(\frac{Z}{z_c}\right)/\ln\left(\frac{10}{z_c}\right)$ where V_{10} is windspeed at 10 m and z_c is the roughness length (generally ≈ 0.1 m in flat areas) where $V = 0$. Available data were extracted from the online data base "Weather Underground" (Weather Underground, 2021) during a period of maximum 20 years (2001-2020) with a minimum of 10 years (2011-2020) depending on data availability (Table 1).

Table 1

Dew yields have been computed from Eq. 2 using standard meteorological databases extracting air and dew point temperatures (T_a and T_d, °C), relative humidity (RH, %), wind speed (km.h^{-1} to be transformed in m.s^{-1}), wind direction (sectors), absolute pressure (hPa) and sky cover. An hourly time-step for measured data is accessible except for Oranjemund

and Luderitz (Namibia) where two time-steps are available (Oranjemund: 6 h. on 2005-2014 and 3 h. on 2014-2020); Luderitz (6 h. on 2006-2012 and 3 h. on 2012-2020).

Wind direction values in degrees have been computed from wind direction sectors (N, NNE, NE, E, ESE, SE, S, etc.) using a standard law of proportionality: 0° for north, 180° for south and calculation of all intermediate values with respect to these references.

The sky cover was considered variable if it varies by one or more of the reported values (CLR, FEW, SCT, BKN, or OVC) during the period of observation (NOAA's national weather service glossary, 2021). Cloud cover in oktas was computed from the nightly observation of sky cover using the correspondence listed in Table SM1 in Supplementary Materials, which was used in a previous work (Muselli et al., 2020). However, cloud cover is sometimes not available at night on some sites (the missing percentage of total values is noted for each site in Table 1). When the sky conditions data are unavailable, we imposed to these sites three possible values, corresponding to the most probable: N = 0, 1 and 3.

Measured rainfall data, available on a daily time step, are extracted from the meteorological data base (Infoclimat database, 2021). All data are obtained for the same stations as used for dew calculation except for Swakopmund where the rainfall data of Walvis Bay are used (both sites are only 25 km apart).

2.4. Kriging maps

Kriging methodologies are mainly used for mapping spatial distribution of a given variable. The classical algorithm is presented in Appendix 2. Belkiri et al. (2020) use Kriging to study ground water composition. Tomaszkiewicz et al. (2016) propose ordinary Kriging to develop

dew maps integrating projected climate changes in the Mediterranean basin. Martinez et al. (2017) present median polish Kriging (MPK) for space-time analysis of monthly precipitation in Colombia. Pue et al. (2021) introduce a Kriging-based Gaussian process for the evaluation for the prediction of soil water retention in tropical and temperate climates. Other studies combine Kriging models for the estimation of rainfall with Lagrangian (Amani et Lebel, 1997) or Bayesian (Lima et al., 2021) approaches.

3. Results

3.1. Evolution

For each site, dew (subscript $i = d$) and rain (subscript $i = r$) monthly yields h_i (mean, min, max in mm) are computed. Annual dew yield (mm) is deduced by adding the monthly h_i:

$$H_i = \sum_{t=1}^{12} h_i(t) \quad (4)$$

In order to estimate the evolution, monthly dew yields can be fitted by a linear regression on the measured period:

$$h_i(t) = \alpha_i t + h_{i,0} \quad (5)$$

With t in month, the coefficient $\alpha_i = dh_i/dt$ represents the monthly evolution rate.

231 3.2. Dew yields

232

233 3.2.1. Data description

234 Mean, minimum and maximum dew yields are calculated on monthly and yearly time bases
235 and reported in Table SM2 in Supplementary Materials. The calculated annual dew yields
236 show significant variations depending on the sites studied even within the same country (Fig.
237 2 and Table SM2).

238 In Namibia, the sites on the west coast (Walvis Bay, Luderitz, Swakopmund and
239 Oranjemund) benefit from high dew yields (> 10 $mm.yr^{-1}$) mainly explained by the high
240 humidity due to the vicinity of the Atlantic Ocean. For example, mean dew yields in the range
241 12.6 to 38.2 $mm.yr^{-1}$ (for $N_{missing}$ = 0, 1, 3) have been obtained in Swakopmund and Walvis
242 Bay, located near the Namib national Park, corresponding to mean monthly dew yields
243 between 2.8 and 6.9 mm. For both stations, dewy days represent between 79.1 (Swakopmund,
244 N = 3) and 85.8% (Walvis Bay, N = 0) of the year. On the other hand, the stations established
245 in the interior of the country suffer from very low annual dew yield (< 5 $mm.yr^{-1}$). For
246 example, Eros, Keetmanshoop and Ondangwa, respectively located at about 250 and 350 km
247 from the ocean, exhibit annual dew yields less than 4.9 mm. In Keetmanshoop, monthly dew
248 yields are very weak with a mean of 0.1-0.3 mm and a monthly maximum of up to 1.8 mm.
249 For Eros and Keetmanshoop, only 10-20% of the days are dewy (min = 8.7% and max =
250 18.4%), while for Ondangwa it is 25% or even 15% (N = 0 for missing data) or even one day
251 a week in the most unfavorable case (N = 3 for missing data).

252 The situation is more homogeneous in Botswana. The mean annual yields are between 6.9 and
253 16.2 mm depending on the sites (min = 1.8-6.6 mm and max = 16.5-26 mm), with monthly
254 yields averaging between 0.6 and 1.4 mm (min = 0 mm and max = 4.2-5.9 mm).

Except in Upington (mean < 5.5 mm), located in the northern Cape Province of South Africa on the banks of the Orange River, and Mahikeng, near to the Bostwana frontier (mean < 9.8 mm), all the country exhibit mean annual dew yields more than 15 mm. For example, Cape Town, Port Elizabeth and George cities, on the south coast, or Wonderboom and Bram Fischer (near respectively Pretoria and Johannesburg), present averaged annual dew yields of more than 18.3 mm, and up to 27 mm. Whereas the maximum monthly dew yields do not exceed 4.7 mm in Upington and Mahikeng, the other cities present monthly dew yields larger than 4.5 mm, and up to 7.7 mm.

The spatial distribution of dew yields was determined by Kriging (Fig. 2, for N = 0, 1, 3 for missing data). Maps of mean annual dew yields are presented in (Figs 2abc). As expected and described in the literature (Henschel et al., 2007; Soderberg, 2010), dew exhibits the highest yields along the west coast of Namibia corresponding to the Namib desert. This desert represents about 81 000 km² and stretches over 1,500 km along a 80 to 160 km wide north-south coastal strip along the Atlantic Ocean. One also clearly observes the decrease in yields inland, especially from the central plateau towards the desert of Kalahari representing a surface of 900 000 km² with 600 000 km² in Namibia. However, one notes that in this critical areas, monthly dew yields can reach - mean and maximal values up to 2-3 mm and 6-8 mm, respectively. Note that the biocrust sites are located in regions of moderate dew yield.

More generally, there is a tendency to see a decrease in dew yield with increasing distance from the oceans, located W, E and S. A clear decrease in nocturnal RH from west to east is obvious (Fig. 2d), with the largest dew yields (Fig. 2c) corresponding to the regions of highest RH.

279 Figure 2

280

281 3.2.2. Evolution map 2001 - 2020

282 In Fig. SM1 (Supplementary Materials) are plotted the evolution of the summed value of dew
283 yield, $\mathrm{sum}(h_d) = \int_{t_0}^{t} h_d dt$ on a monthly basis, with t_0 the starting year (see Table 1). The
284 dew rate is either nearly constant during the period (Swakopmund, Walvis Bay, Eros,
285 Keetmanshoop, Cape Town, Port Elizabeth, Gaborone, Bram Fischer) or increases (Luderitz,
286 Oranjemund, Upington, Shakawe, George, Maun, Mahikeng, Wonderboom) after year 2010.
287 One will see in Section 3.3 that the year 2010 is also the year where rainfalls significantly
288 decrease.

289

290 By considering the period where meteorological data are available on all sites (2011-2020),
291 one can determine the evolution of the average yield at any point in the study area by
292 subtracting annual dew yields between years 2020 and 2011. Figure 3 shows the difference
293 $\Delta h_d = h_d(2020) - h_d(2011)$. One sees that the evolution is different according to the locations.
294 Although dew decreases in two places where it was the most abundant (SW and NE to a lesser
295 extent), it increases in the NW (Ondangwa, Eros) where dew was the lowest. A noticeable
296 increase is seen in *N* (Maun, Shakawe) and SE regions (Bram Fischer). One notes that the
297 biocrust sites are mostly located in regions of null or moderate dew decrease.

298

299 Figure 3

300

3.3 Rainfall

3.3.1. Data description

Table 2 and Fig. 4 present annual and monthly mean, min and max rainfall extracted from Infoclimat database (2021) for the studied period (sites: See Table 1). From a general point of view, rain decreases towards W and N. As described below, cities located at the Namib desert exhibit lower rain precipitations: 13.4 mm in Swakopmund and Walvis Bay (i.e. 1% of rainfall events by year) and in a lesser extent, Oranjemund with a mean annual rainfall of about 42 mm (i.e. 5% of rainfall events by year). In these areas, precipitations are very erratic, with no rain for several months and few intense precipitations events. In the inland, rainfall is slightly more abundant with annual averages of 115, 189 and 306 mm for Keetmanshoop, Ondangwa and Eros, respectively. Although these areas can exhibit months without any rain, the monthly averages are greater than 10 mm. However, one notes that less than 11% of the days of the year are rainy days (10.9%, 5.3% and 3.7% in Eros, Ondangwa and Keetmanshoop, respectively).

For Botswana, the situation is more homogenous, with a mean rainfall of 463.2 mm observed in the four cities of Gaborone, Maun, Francistown and Shakawe. With one or two months during the year without rain, this region present mean regular monthly rainfall of about 39 mm, with 13.4 % of the days being rainy.

South Africa exhibits a contrasted behavior. The regions located along the ocean in the south and south east of the country have heavy rainfall with annual amounts greater than 500 mm (Mahikeng, Cape Town, George, Port Elizabeth, Bram Fischer, Wonderboom), with up to 715 mm in George (18 - 31% of the year are rainy days). Monthly averages are important with a mean of about 49.6 mm (23.5% rainy days in the year). Upington is an exception, located

325 further west of the country, but with lower rainfall (285 mm.year^{-1} with a mean of 23.8
326 mm.month^{-1}).

327 One notes a marked decrease in precipitation during the 20 years period, all sites show ($\alpha(h_r)$
328 < -0.2), particularly in Eros and Ondangwa in Namibia, the 4 cities of Bostwana, and George
329 and Bram Fisher in South Africa. Coastal sites in Namibia (Oranjemund, Luderitz,
330 Swakopmund and Walvis Bay) show a smaller decrease ($\alpha(h_r) \approx 0$). When looking at Fig.
331 SM1 in Supplementary Materials (summed values of h_r), one realizes that the main change in
332 rainfalls occurred in 2010. It is from this year that a gradual change in rain can be observed.

333 The rainfall repartition presented in Table 2 is confirmed by the Kriging map obtained for the
334 annual mean rainfall (Fig. 4a). Rainfall increases markedly from west to east (0-200 mm at
335 the Atlantic coast to 600 to 700 measured at the south-east of South Africa). The same trend is
336 observed with the monthly mean and maximum rainfall volumes (Figs. 4bc). The monthly
337 average varies from 0 to 20 mm (W) to 50 to 60 mm (SE).

338

339 Table 2

340

341 Figure 4

342

343 3.3.2 Evolution map

344 By subtracting the precipitation values between years 2020 and 2011 one can map (Fig. 5) the
345 difference $\Delta h_r = h_r$ (2020) – h_r (2011). Although the mean precipitation decreases, the
346 evolution is different depending on the locations. Rain mainly decreases in the north regions
347 (Maun, Shakawe, Eros), where dew was seen to increase during the same time period (Fig. 3).

A small zone in south west (Cape Town, Oranjemund) exhibits a precipitation increase. It is worthy to note that the biocrust zones are mostly in the regions that experienced a decrease in rain.

Figure 5

3.4 Correlation between dew and rain yields

The occurrence of dew is related to the presence of atmospheric high humidity. Some correlations therefore exist between the frequency and amplitude of rain and the amplitude of dew yields. Two kinds of correlation can occur, a temporal correlation, where dew forms after rain events, which have increased the atmosphere RH, and an amplitude correlation. Both correlations are studied in the following.

3.4.1. Temporal correlation

The temporal correlation between rainfall and dew yield is evaluated by a correlation coefficient r between the daily rainfall, $h_r(t)$, and the time-shifted daily dew yield, $h_d(t+\tau)$, estimated at the same location. The delay time τ corresponds to the previous and next days of time t and is counted in days in the interval [-31, +31] . The covariance between $h_d(t+\tau)$ and $h_r(t)$ is calculated as:

$$C[h_r(t), h_d(t+\tau)] = \frac{1}{n}\sum_{j=1}^{n}\left(h_{r,j}(t) - \overline{h_r}\right)\left(h_{d,j}(t+\tau) - \overline{h_d}\right) \quad (6)$$

With $\sigma_{h_r}, \sigma_{h_d}$ the rain and dew standard deviation, respectively, one infers the correlation coefficient:

$$r[h_r(t), h_d(t+\tau)] = \frac{C\{h_r(t), h_d(t+\tau)\}}{\sigma_{h_r}\sigma_{h_d}} \quad (7)$$

Considering that $-1 < r < 1$, a negative correlation leads to an opposite evolution of h_r and h_d, a positive correlation corresponds to the two variables moving in the same trend and $r \to 0$ means that both variables are not correlated.

The *r* correlation plots for each meteorological site according to the three *N* scenarii are reported in Fig. 6. One observes the following:

(i) For $\tau < 0$, no correlations between dew and rain amplitudes are observed (mostly $r < 0.05$). It means that a rain event at a given day does not explain of dew events a few days earlier.

(ii) For $\tau = 0$, all curves present negative values for *r*, with amplitude in the range [-0.3 – 0.1]. This is due to the fact that, in the calculation of the dew yields in Section 2.1, one had to discard the days with rain.

(iii) For $\tau > 0$, some correlation can be observed for $\tau \leq 3$ days. For the Eros and Keetmanshop sites, $r = 0.29$ ($N = 3$) and $r = 0.18$ ($N = 1$). For Mahikeng and Upington, $r = 0.12$ ($N = 1$) and $r = 0.13$ ($N = 0$). To a lesser extent, for Bram Fischer $r = 0.097$ for $N = 1$. These values thus indicate a weak but real positive correlation between rain and dew events. It means that, due to the increase of atmosphere humidity after rain events, dew events are more likely to be observed one to three days after rainfalls.

The correlation dew-rain is most noticeable (Ondangwa, Eros, Keetmanshop; Upington, Mahikeng, Bram Fisher) when the distance from the ocean increases, the atmosphere RH then

decreases (see Fig. 2d). In contrast, for stations close to the coast in arid climate (distance < 15 km) and with low annual rainfall (H_r < 50 mm) but large RH, such as Luderitz, Oranjemund, Swakopmund and Walvis Bay, the correlation is very low regardless of the τ value. For the cities of Cape Town, Port Elizabeth and George, presenting a more temperate climate, the correlation shows at most a weak increase for τ < 4 to 5 days (with r < 0.1). All these sites have an altitude below 200 m.

Whatever is the *N* scenario, for altitudes between 800 m and 1700 m asl and > 200 km away from the ocean, the correlation is clearer with values of r showing a steady increase at Eros (1700 m asl, 266 km from the ocean), Keetmanshoop (1069 m asl, 285 km from the ocean). Ondangwa (1099 m asl, 385 km from the ocean) and Bram Fischer (1349 m asl, 418 km from the ocean) show a correlation with r > 0.1, respectively for τ = 2 and 3. For the other mountainous stations, the correlation coefficients exhibit values that does not exceed 0.1, with τ = 5 for Gaborone (r = 0.0532) or τ = 3 for Maun (r = 0.0665).

Figure 6

3.4.2. Summed dew and rain yields

One now investigates the correlation between the cumulative dew and rain monthly yields, $\mathrm{sum}(h_d) = \int_{t_0}^{t} h_d dt$ and $\mathrm{sum}(h_r) = \int_{t_0}^{t} h_r dt$, respectively, with t_0 in Table 1. Each data point will thus correspond to a monthly mean value. For each month, a ratio $a(t)$ is calculated:

$$a(t) = \frac{[\mathrm{sum}(h_d)]_t}{[\mathrm{sum}(h_r)]_t} \quad (8)$$

In Fig. 7a the $\mathrm{sum}(h_d)$, the $\mathrm{sum}(h_r)$ and their ratio $a(t)$ for two sites (Upington and Cape Town sites) are reported (at small times the dispersion is large because the smoothing effect of the summation is still weak). In Cape Town, both rain and dew amounts are nearly linear during the research period, with a decrease in rainfall rate after 2010 while the dew rate remains constant. In Upington, one observes a decrease in the rain amount and an increase in the dew amount after 2010. For sake of comparison in the whole time period, the data (Fig. 7b) can be fitted to a mean constant value

$$a(t) = a_0 \quad (9)$$

Figure 7

The values of a_0 according to the three N scenarios are summarized in Table 3. Taking into account all stations, the parameter a_0 shows a large variability: $\overline{a_0} = 0.4 \pm 0.8$ ($N = 0$), $\overline{a_0} = 0.3 \pm 0.6$ ($N = 1$) and $\overline{a_0} = 0.15 \pm 0.27$ ($N = 3$). This variability is due to the small number and erratic character of the precipitations in arid areas. When the very small quantities of rain at these sites (Namib Desert: Oranjemund, Luderitz, Swakopmund and Walvis Bay) are removed, the variability of values becomes much smaller ($\overline{a_0} = 0.022 \pm 0.008$ ($N = 0$), $\overline{a_0} = 0.020 \pm 0.009$ ($N = 1$) and $\overline{a_0} = 0.017 \pm 0.011$ ($N = 3$)).

Table 3

436

437 The parameter $\overline{a_0}$ is mapped by the Kriging method in Fig. 8. One can clearly observe the
438 increasing importance of dew in the total precipitations along the Namibian coast and more
439 generally the dependence of *a* on longitude. It corroborates the fact that the distance from the
440 ocean, which controls the atmosphere RH (see Fig. 2), is the important parameter for the
441 formation of dew. Toward the west, dew increases (Fig. 2) and rain decreases (Fig. 4), leading
442 to an increase in *a*.

443

444 Figure 8

445

446 The variation of the ratio *a* between 2020 and 2011 is reported in Fig. 9. One verifies the
447 general increase of the contribution of dew with respect to rain, especially towards west.

448

449 Figure 9

450

451 3.5 Time period of events

452 Because the frequency or time period between rain events is also an important parameter,
453 which in itself can control the biocrust growth, we investigate below this parameter for rain
454 only, dew only and dew plus rain. For that purpose, one considers the histogram of rain, dew
455 and rain plus dew events (Fig. 10) where two important parameters can be extracted, the mean
456 time period between events, θ_0 (in days) and the maximum time period, θ_M (in days).

457

458 Figure 10

459

460

461 The evolution of θ_0 and θ_M can be then considered (Fig. SM2) and maps of mean values can
462 be drawn for the considered period (Fig. 11), with the difference between 2011 and 2020
463 values (Fig. 12). Some curves are interrupted due to the lack of data.

464

465

466 One first notes from Figs. 10 and SM2 (in Supplementary Materials) that the number of
467 events is larger for dew than for rain. In addition, the timescale for mean and maximum time
468 period between events is much larger for rain than for dew, a difference which can reach two
469 orders of magnitudes. It results from the above observations that the dew events will
470 determine the behavior of the dew + rain time period (see Fig. SM2, Figs 11– 12).

471

472 Figure 11

473

474 When comparing the maps of dew and rain mean annual times (Fig. 11) and dew and rain
475 amplitudes (Figs. 2 and 4), one observes a strong correlation between the zones of large times
476 and low yield, and short times and high yield. This simply means that large water yields
477 correspond to frequent dew or rain events.

478 The evolution of the mean and maximum time period between 2001 and 2020 (Fig. SM2)
479 show that mean and maximum time periods evolve about the same way. The times keep

480 nearly constant over the whole period for dew, noting a slight decrease after 2010. Dew times
481 are well correlated with the dew yield amplitude, which remains constant or weakly increases
482 in the same period (Fig. SM1 in Supplementary Materials). In contrast, for rain, while the
483 times keep constant between 2001 and 2010, the times increase after 2010. This evolution
484 corresponds well with the decrease of rain amplitude (Fig. SM1).

485 The maps of evolution for the period 2011 – 2020 concerning the differences in rain, dew and
486 rain + dew times are reported in Fig. 12. The evolution mean and maximum times are
487 qualitatively similar to the evolution of the rain and dew amplitudes (Figs. 3 and 5). The
488 evolution of rain + dew times rather follows the dew evolution, as expected from the fact
489 noted above that the dew events mostly determine the behavior of the dew + rain times.

490

491 Figure 12

492

493 **4. Discussion and relation with biocrust**

494

495 4.1. Dew height dependence

496 Biocrust forms at the ground level while the calculation of Section 2.1 deals with a 30° tilted
497 condenser at 1 m off the ground. Dew condensation can vary for three reasons. (i) RH can be
498 height dependent. This is the case if wind speed is near zero and soil is wet, for instance after
499 a rain event. (ii) Air flow depends on height, and then, the heat and mass exchange with the
500 surrounding air. The variation of air flow velocity is known to follow a log dependence above
501 a roughness length z_c (see Section 2.3) where air flow velocity is zero. In addition to the
502 forced air flow induced by wind, there exists a natural convection induced by the substrate

503 temperature colder than ambient air, with typical velocity 0.6 $m.s^{-1}$ (Beysens et al., 2005; Clus
504 et al., 2009). The log dependence of the windspeed and the presence of natural convection
505 make the heat exchange coefficient and then the mass diffusion coefficient, which determines
506 the condensation yield, depend weakly of windspeed for values below ~ 1 $m.s^{-1}$ (measured at
507 the standard height of 10 m). It results a weak dependence of condensation with height for
508 such windspeeds, making the calculation of Section 2.1 valid at the ground level.

509 For larger windspeeds, the heat exchange coefficients will be larger, decreasing the dew yield.
510 The latter will be then larger at the ground level and the calculation of Section 2.1 will be a
511 conservative value.

512

513 4.2. Comparison with direct dew yield measurements

514 The calculated dew yields can be compared with previous works available in the literature.
515 Baier (1966) reported dew and rainfall measurements from a weather station set at
516 Potchefstroom (inclined cross in Fig. 2), located in the vast interior plateau of South Africa
517 (26°44' S, 27°05' E, 1352 m asl), about 160 km from the Wonderboom site. During the
518 period 1957-1958, the annual percentage of dew days was 45.7% (Wonderboom: 65.5%) with
519 a mean annual dew amount of 12.6 mm (Wonderboom: 19.9 mm). The values in
520 Wonderboom are slightly larger, but the time is earlier and we will see in the next Section that
521 the general tendency is a positive dew yield evolution.

522 Dew collection were also carried out in 2006 by Henschel et al. (2007) at Gobabeb (Namib
523 desert, 23°33.704 S, 15°02.466 E, right cross in Fig. 2) in Namibia's Central Namib desert,
524 situated about 84 km from Walvis Bay and 110 km from Shakopmund. The site elevation is
525 406 m. Only a few data were collected on a specially-designed 1 m^2 passive dew collector. In
526 July 2006, 3.3 mm of dew water was collected (12 dew days), 1.2 mm in August (10 dew

527 days), and 1.5 mm in September (10 dew days). Meteo data at Walvis Bay and Shakopmund
528 are, however, available only between 2010 and 2020. In these cities, the calculated annual
529 mean in July, August and September are nearly the same: 2.6 mm (July), 2.2 mm (August)
530 and 2.2 mm (September) (N = 0), 1.2 mm, 1.8 mm and 1.7 mm (N = 1) and 0.7 mm, 0.9 mm
531 and 0.9 mm (N = 3). Although not determined at the same dates, these values compare
532 relatively well with the above measured values of 3.3 mm (July), 1.2 (August) and 1.5 mm
533 (September).

534 Between July 2008 and June 2009, Soderberg (2010) measured a greater amount of dew at
535 Gobabeb, with 143 yearly dew events. The corresponding volume was 12.3 mm, which
536 compares relatively well with the Walvis Bay and Shakopmund data for the same year: 21
537 mm (N = 0), 15.8 mm (N = 1), 7 mm (N = 3).

538

539 4.3 Variation in rain precipitation

540 As mentioned in Section 3.3, we observed a decrease of precipitation from west to east. All
541 sites present a negative variation in rain precipitation during 2001 to 2020. In particular, the
542 decrease in precipitation is quite noticeable from 2010. In Namibia Lu et al. (2016) also
543 observed a tendency to a diminution of rainfall precipitations. On the Ghaap plateau in west
544 center of South Africa, oscillations of rain precipitations have been already noted by Tfwala et
545 al. (2018) by analyzing interannual rainfall variability on the Ghaap plateau. The cycles last
546 about 18 -22 years years in Postmarburg and between 12 and 16 years in Douglas. Another
547 analysis of rainfall in South Africa by Zvarevashe at al. (2018) also concluded to quasi-
548 decadal oscillations. The question whether the decrease we observed since 2010 is related to
549 these oscillations or to the global climate change remains thus open.

550

4.4 Water availability and biocrust distribution

As outlined in the Introduction, the amount of rain and dew are considered as the main factors which influence the growth of biocrust (see e.g. Pan et al., 2010; Zhuang and Zhao, 2017; Ouyang et al.; 2017; Kidron, 2020; Li et al., 2021a, b). However, the frequency of rain events (longest period of drought) is the main factor according to Büdel et al. (2009). Although there are no studies concerning the effect of frequency of dew events, one can reasonably assume that this parameter also matters.

Frequency of events and their amplitude are strongly correlated (see Section 3.5), the regions of large dew or rain amplitudes corresponding to the regions of small dew or rain time periods. Both criteria (amplitude, time frequency) should thus correspond in the studied regions to the same characteristics favoring biocrust growth.

The evolution between 2001 and 2020 is seen to exhibit two regimes, one from 2001 to 2010, where all parameters (dew and rain amplitude, dew and rain frequency) keep nearly constant. The second regime, from 2010 to 2020, corresponds to a neat decrease of rain amplitude and frequency of events, while dew amplitude and frequency either keeps constant or slightly increase. As far as rain is concerned, it should result in a decrease of biocrust growth. However, dew yield is nearly constant or increases after 2010. We are not aware of drastic changes in the distribution of biomass of biocrusts during the 2001-2020 period. This may be attributed to the increase of dew amplitude and frequency, which should act to compensate for the decrease in rain precipitation.

5. Conclusion and trends for the future

The determination of dew yield using a physical model and rainfall data from 18 meteorological stations in Namibia, Botswana and South Africa in the period 2001-2020

allow clear tendencies to be evaluated. Dew decreases from the East, South, West coasts following the decrease in RH decrease, and rainfalls diminish toward the West and North. A noticeable decrease in rain precipitations after 2010 and a corresponding rise in dew yield are noted. It results in a steady increase of dew contribution with respect to rain after 2010. In addition, a clear increase in dew for three days in average after rainfall is observed in the arid regions where the humidity is low. These results are corroborated with the frequency of dew and rain events, which are closely correlated with dew and rain yields.

The effect on biocrust is to show zones with less rain but with increasing dew water. As far as rain is concerned, one therefore should expect a decrease of biocrust growth. However, dew yield is nearly constant or even increases slightly after 2010, which could possibly compensate the rain decrease as we are not aware of drastic changes in the distribution of biomass of biocrusts during the 2001-2020 period.

The observed evolution, studied from 2001, exhibits a change after 2010. The question whether this decrease is related to oscillations or to a general tendency due to the global climate change remains open. A more precise scenario will need the use of climate change models as was done by Tomaszkiewicz et al. (2016). We plan such a study in a near future.

Acknowledgments

We gratefully thank G. Kidron for his valuable remarks.

References

Agam, N., Berliner, P.R., 2006. Dew formation and water vapor adsorption in semi-arid environments—A review. J. Arid Environ., 65, 572–590.

598

599 Aguirre-Gutiérrez, C.A., Holwerda, F., Goldsmithc, G.R., Delgado, J., Yepez, E., Carbajal,
600 N., Escoto-Rodríguez, M., Arredondo, J.T., 2019. The importance of dew in the water balance
601 of a continental semiarid grassland. J. Arid Environ., 168, 26-35.

602

603 Amani, A., Lebel, T., 1997. Lagrangian Kriging for the estimation of Sahelian rainfall at
604 small time steps. J. Hydrol., 192, 125-157.

605

606 Baier, W., 1966. Studies on dew formation under semi-arid conditions. Agric. Meteorol., 3,
607 103-112.

608

609 Bargaoui, Z., Chebbi, A., 2009. Comparison of two Kriging interpolation methods applied to
610 spatiotemporal rainfall. J. Hydrol., 365, 56-73.

611

612 Belkiri, L., Tiri, A., Mouni, L., 2020. Spatial distribution of the groundwater quality using
613 Kriging and Co-Kriging interpolations. Groundw. Sustainable Dev., 11, 100473.

614

615 Beysens, D., 2016. Estimating dew yield worldwide from a few meteo data. Atmos. Res., 167,
616 146–155.

617

618 Beysens, D., Muselli, M., Nikolayev, V., Narhe, R., Milimouk, I., 2005. Measurement and
619 modelling of dew in island, coastal and alpine areas. Atmos. Res., 73, 1–22.

Büdel, B., Darienko, T., Deutschewitz, K., Dojani, S., Friedl, S., Mohr, K.I., Salisch, M., Reisser, W., Weber, B. 2009. Southern African biological soil crusts are ubiquitous and highly diverse in drylands, being restricted by rainfall frequency. Microb. Ecol., 57:229–247.

Cano-Díaz, C., Mateoa, P., Muñoz-Martína, M.A., Maestre, F.T., 2018. Diversity of biocrust-forming cyanobacteria in a semiarid gypsiferous site from Central Spain. J. Arid Environ., 151, 83-89.

Chen, N., Yu, K., Jia, R., Teng, J., Zhao, C., 2020. Biocrust as one of multiple stable states in global drylands, Sci. Adv., 6, eaay3763.

Clus, O., Ouazzani, J., Muselli, M., Nikolayev ,V. S., Sharan, G. Beysens, D., 2009. Comparison of Various Radiation-cooled Dew Condensers Using Computational Fluid Dynamics. Desalination, 249, 707–712.

Goovaerts, P., 1997. Geostatistics for natural resources evaluation. Oxford university press, New York, 500p.

Henschel, J., Siteketa, V., Berkowicz, S.M., Beysens, D., Milimouk-Melnytchouk, I., Muselli, M., Heusinkveld, B.G., Jacobs, A.F.G., 2007. Dew Occurrence and Collection in Gobabeb,

641 Central Namib Desert. Proc. 4th Conf. on Fog, Fog Collect. and Dew (La Serena, Chile, 23-
642 27 July 2007), p. 251.

643

644 Infoclimat database, 2021. https://www.infoclimat.fr

645

646 Jacobs, A.F.G., Heusinkveld, B.G., Berkowicz, S.M., 2002. A simple model for potential
647 dewfall in an arid region. Atmos. Res., 64, 285-295.

648

649 Jones, A., Breuning-Madsen, H., Brossard, M., Dampha, A., Deckers, J., Dewitte, O., Gallali,
650 T., Hallett, S., Jones, R., Kilasara, M., Le Roux, P., Micheli, E., Montanarella, L., Spaargaren,
651 O., Thiombiano, L., Van Ranst, E., Yemefack, M., Zougmoré R., (eds.), 2013. Soil Atlas of
652 Africa. European Commission, Publications Office of the European Union, Luxembourg.
653 176p.

654

655 Kidron, G.J., 2019. The enigmatic absence of cyanobacterial biocrust from the Namib fog
656 belt: Do dew and fog hold the key? Flora, 257, 151416.

657

658 Kidron, G.J., Tal, S.Y., 2012. The effect of biocrust on evaporation from sand dunes in the
659 Negev Desert. Geoderma, 179-180, 104-112.

660

661 Kidron, G.J., Kronenfeld, R., 2020. Assessing the likelihood of the soil surface to condense
662 vapour: The Negev experience. Ecohydrol., 13, e2200.

Kool, D., Agra, E., Drabkin, A., Duncan, A., Fendinat, P.P., Leduc, S., Lupovitch, G., Nambwandja, G., Ndilenga, N.S., Nguyễn Thi, T., Poodiack, B., Sagi, L., Shmuel, Y., Maggs-Kölling, G., Marais, E., Pinshow, B., Turner, J.S., Agam, N., 2021. The overlooked non-rainfall water input sibling of fog and dew: Daily water vapor adsorption on a !Nara hummock in the Namib Sand Sea. J. Hydrol., 598, 126420D.

Lepioufle, J.M., Leblois, E., Creutin, J.D., 2012. Variography of rainfall accumulation in presence of advection. J. Hydrol., 464-465, 494-504.

Li, S., Bowker, M.A., Xiao, B., 2021a. Biocrust enhance non-rainfall water deposition and alter its distribution in dryland soils. J. Hydrol., 595, 126050.

Li, S., Xiao, B., Kidron, G.J., 2021b. Moss-dominated biocrust enhance water vapor sorption capacity of surface soil and increase non-rainfall water deposition in drylands. Geoderma 388, 114930.

Lima, C.H.R., Kwon, H.H., Kim, Y.T., 2021. A Bayesian Kriging model applied for spatial downscaling of daily rainfall from GCMs. J. Hydrol., 597, 126095.

683 Lu, X., Wang, L., Pan, M., Kaseke, K.F., Li, B., 2016. A multi-scale analysis of Namibian
684 rainfall over the recent decade – comparing TMPA satellite estimates and ground
685 observations. J. Hydrol. Reg. stud., 8, 59-68.

686

687 Martinez, W.A., Melo, C.E., Melo, O.O., 2017. Median Polish Kriging for space–time
688 analysis of precipitation. Spat. Stat., 19, 1-20.

689

690 Museli, M., Clus, O., Ortega, P. Milimouk, I., Beysens, D. 2020. Physical, chemical and
691 biological characteristics of dew and rain water during the dry oceans on of tropical islands.
692 Atmos., 12, 69.

693

694 New, M., Hulme, M., Jones, P., 2000. Representing Twentieth-Century Space–Time Climate
695 Variability. Part II: Development of 1901–96 Monthly Grids of Terrestrial Surface Climate. J.
696 Climatol., 12, 829-856.

697

698 NOAA. 2021. Available online: https://www.forecast.weather.gov (accessed on 13 February
699 2021).

700

701 Ouyang, H., Lan, S., Yang, H., Hu, C., 2017. Mechanism of biocrust boosting and utilizing
702 non-rainfall water in Hobq Desert of China. Appl. Soil Ecol., 120, 70-80.

703

704 Pal Arya, S., 1988. Introduction to Micrometeorology. Acad. Press, San Diego, 307p.

Pan, Y., Pan, Wan, X., Zhang, Y., 2010. Dew formation characteristics in a revegetation-stabilized desert ecosystem in Shapotou area, northern China. J. Hydrol., 387, 265–272

Pue, J.D., Botula, Y.D., Nguyen, P.M., Meirvenne, M.V., Cornelis, W.M., 2021. Introducing a Kriging-based Gaussian Process approach in pedotransfer functions: Evaluation for the prediction of soil water retention with temperate and tropical datasets. J. Hydrol., 597, 125770.

Raggio, J., Green, A., Pintado, A., Sancho, L.G., Büdel, B., 2021. Functional performance of biocrust across Europe and its implications for drylands. J. Arid Environ., 186, 104402.

Rahmawati, N., 2020. Space-time variogram for daily rainfall estimates using rain gauges and satellite data in mountainous tropical Island of Bali, Indonesia (Preliminary Study). J. Hydrol., 590, 125177.

Railsback, L.B., Kraft, S., Liang, F., Brook, G.A., Marais, E., Cheng, H., Edwards, R.L., 2019. Control of insolation on stalagmite growth, rainfall, and migration of the tropical rain belt in northern Namibia over the last 100 kyr, as suggested by a rare MIS 5b-5c stalagmite from Dante Cave. Palaeogeogr., Palaeoclimatol., Palaeoecol., 535, 109348.

726 Soderberg, K.S., 2010. The role of fog in the ecohydrology and biogeochemistry of the Namib
727 Desert, MSc, University of Cape Town, Department of Environmental Sciences, University of
728 Virginia.

729

730 Tomaszkiewicz, M., Najm, A., Beysens, D., Alameddine, I., Zeid, EB, El-Fadel, M., 2016.
731 Projected climate change impacts upon dew yield in the Mediterranean basin. Sci. Total.
732 Environ., 566-567, 1339-1348.

733

734 Trosseille, J., Mongruel, A., Royon, L., Beysens, D., 2021. Effective surface emissivity
735 during dew water condensation. Submitted.

736

737 Tfwala, C.M., Van Rensburga, L.D., Schallb, R., Dlamini, P., 2018. Drought dynamics and
738 interannual rainfall variability on the Ghaap plateau, South Africa, 1918–2014. Phys. Chem.
739 Earth, 107, 1-7.

740

741 Van de Beek, C.Z., Leijnse, H., Torfs, P.J.J.F., Uijlenhoet, R., 2012. Seasonal semi-variance
742 of Dutch rainfall at hourly to daily scales. Adv. Water Resour., 45, 76-85.

743

744 Weather-and-Climate database, 2021. https://weather-and-climate.com

745

746 Weather Underground database, 2021, https://www.wunderground.com

747

748 Yao, X., Xia, B., Kidron, G.J., Hu, K., 2019. Respiration rate of moss-dominated biocrust and
749 their relationships with temperature and moisture in a semiarid ecosystem. Catena, 183,
750 104195.

751

752 Zhuang, Y., Zhao, W., 2017. Dew formation and its variation in Haloxylon ammodendron
753 plantations at the edge of a desert oasis, northwestern China. Agric. For. Meteorol., 247, 541-
754 550.

755

756 Zvarevashe, W., Krishnannair, S., Sivakumar, V., 2018. Analysis of Austral Summer and
757 Winter Rainfall Variability in South Africa Using Ensemble Empirical Mode Decomposition.
758 IFAC paperOnline, 51-5, 132-137.

759

760

761 **Appendix 1 – Dew yield calculation**

762 We give below an example of determination of dew yield from Section 2.1. The model (Eq. 2)
763 is applied to one night (March 21-22, 2010) in Cape Town (South Africa). Considering the
764 sky nebulosity (N, oktas), the air (T_a, °C) and dew (T_d, °C) temperatures, the relative humidity
765 (RH, %) and the windspeed (V, m.s^{-1}) at 10 meters of the ground, recorded every Δt = 1h., we
766 compute an hourly yield h_i (mm) corresponding to evaporation ($h_i < 0$) or condensation ($h_i >$
767 0) events. By discarding evaporation ($h_i < 0$) and rain events, the cumulative dew yield h for
768 each night is computed. For the studied night, h = 0.185 mm.

769

Date (dd/mm/aaaa)	Hour (hh:mm)	N (oktas)	V (m/s)	T_a (°C)	RH (%)	T_d (°C)	T_d-T_a (°C)	h_i (mm)	$h_i > 0$ (mm)	sum(h_i) (mm)
21/03/2010	12:00	5	6.1	22	69	16	-6	-0.030	0.000	**0.000**
21/03/2010	13:00	5	7.2	23	65	16	-7	-0.035	0.000	**0.000**
21/03/2010	14:00	3	7.8	22	69	16	-6	-0.030	0.000	**0.000**
21/03/2010	15:00	1	7.8	22	69	16	-6	-0.030	0.000	**0.000**
21/03/2010	16:00	1	6.1	22	69	16	-6	-0.030	0.000	**0.000**
21/03/2010	17:00	1	5.6	21	68	15	-6	-0.030	0.000	**0.000**
21/03/2010	18:00	1	4.7	19	83	16	-3	-0.015	0.000	**0.000**
21/03/2010	19:00	0	3.1	18	88	16	-2	0.014	0.014	**0.014**
21/03/2010	20:00	0	0.6	18	88	16	-2	0.014	0.014	**0.027**
21/03/2010	21:00	0	1.9	15	94	14	-1	0.019	0.019	**0.046**
21/03/2010	22:00	0	3.1	14	100	14	0	0.024	0.024	**0.070**
21/03/2010	23:00	0	3.1	17	88	15	-2	0.014	0.014	**0.084**
22/03/2010	00:00	0	3.1	17	88	15	-2	0.014	0.014	**0.098**
22/03/2010	01:00	0	3.1	17	94	16	-1	0.019	0.019	**0.117**
22/03/2010	02:00	0	4.2	17	94	16	-1	0.012	0.012	**0.128**
22/03/2010	03:00	0	5.3	17	100	17	0	0.000	0.000	**0.128**
22/03/2010	04:00	0	3.6	18	94	17	-1	0.018	0.018	**0.146**
22/03/2010	05:00	0	3.1	17	100	17	0	0.023	0.023	**0.170**
22/03/2010	06:00	1	3.6	17	94	16	-1	0.015	0.015	**0.185**
22/03/2010	07:00	1	4.7	18	88	16	-2	-0.010	0.000	**0.185**
22/03/2010	08:00	1	6.7	21	83	18	-3	-0.015	0.000	**0.185**
22/03/2010	09:00	1	7.8	24	69	18	-6	-0.030	0.000	**0.185**
22/03/2010	10:00	1	9.2	25	61	17	-8	-0.040	0.000	**0.185**
22/03/2010	11:00	1	9.2	26	57	17	-9	-0.045	0.000	**0.185**
22/03/2010	12:00	1	10.8	25	65	18	-7	-0.035	0.000	**0.185**

770

Appendix 2 – Kriging method

Kriging is a stochastic spatial interpolation method that predicts the value of a natural phenomenon at non-sampled sites by an unbiased, minimal variance linear combination of observations of the phenomenon at nearby sites. The Kriging tool assumes that the distance or direction between the sample points reflects a spatial correlation that can explain the surface variations. The Kriging tool applies a mathematical function to all points, or certain determined points, located within a specific radius. It determines the output value of each location.

The Kriging tool is particularly suitable for cases where it is known that there is a spatial correlation of distance or a directional deviation in the data. Kriging deduces, by weighting existing readings, the probable values of unmeasured locations. To calculate the interpolated data $\hat{Z}(s_0)$ at a specific location s_0, the general formula of ordinary Kriging (OK) method consists of a weighted sum of the data (Goovaerts, 1997):

$$\hat{Z}(s_0) = \sum_{i=1}^{P} \lambda_i Z(s_i)$$

Here $Z(s_i)$ corresponds to the measured value at the i^{th} location, λ_i the ponderation coefficient to determine and relate to the i^{th} location, s_0 the predicted location and p the number of measured data.

With the Kriging method, the λ_i weighted coefficients are not only based on the distance between the surveyed points and the forecast location, but also on the general spatial

792 organization of the surveyed points. To use the spatial arrangement in the weighing, the
793 spatial autocorrelation is quantified. Thus, in ordinary Kriging, the weighting λ_i depends on
794 the distance from the forecast location and the spatial relationships between the values
795 recorded around it.

796 The experimental semi-variogram can be estimated from point pairs:

$$\hat{\gamma}(h) = \frac{1}{2n(h)} \sum_{i=1}^{n(h)} [Z(s_i) - Z(s_i + h)]^2$$

797 Where

$$n(h) = Card\{(s_i, s_j) / |s_i - s_j| \approx h\}$$

798 with "card" represents the number of elements for the given condition.

799 Classically, estimated semi-variogram are fitted by a spherical variogram model as proposed
800 in previous studies on rainfall spatial estimation (Bargaoui et Chebbi, 2009 ; Lepioufle et al.,
801 2012 ; Van de Beek et al., 2012 ; Rahmawati, 2020).

802

803 **Supplementary materials**

804 We present below supplementary materials for additional calculated data.

805 Figure SM1 reports the evolution of the dew summed values sum(h_d) (dew, mm, full blue
806 line) and the rain summed values sum(h_r) (rain, mm, interrupted red line) for the studied sites.

807 Figure SM2 is concerned with the evolution of the mean time θ_0 (day) and the maximum time
808 θ_M (day) between (a) rain (orange line), dew (blue short interrupted line) and rain plus dew
809 events (green long interrupted line).

Table SM1 gives the correlation between the sky conditions and the cloud cover in oktas according to NOAA.

Table SM2 reports the yearly (H_d) and monthly (h_d) mean, minimum and maximum dew yields calculated from meteorological data.

Figure SM1

Figure SM2

Table SM1

Table SM2

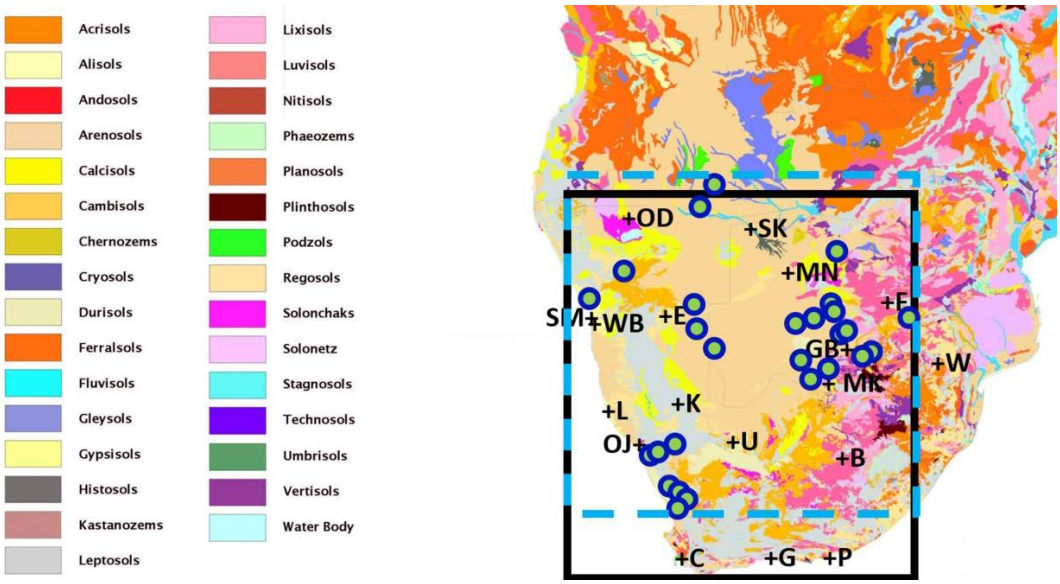

Fig. 1. Map of soils in the studied area (from Jones et al., 2013). Black rectangle and black letters are airport stations. The interrupted blue rectangle corresponds to the biocrust sites (green circles, see Chen et al., 2020).

827

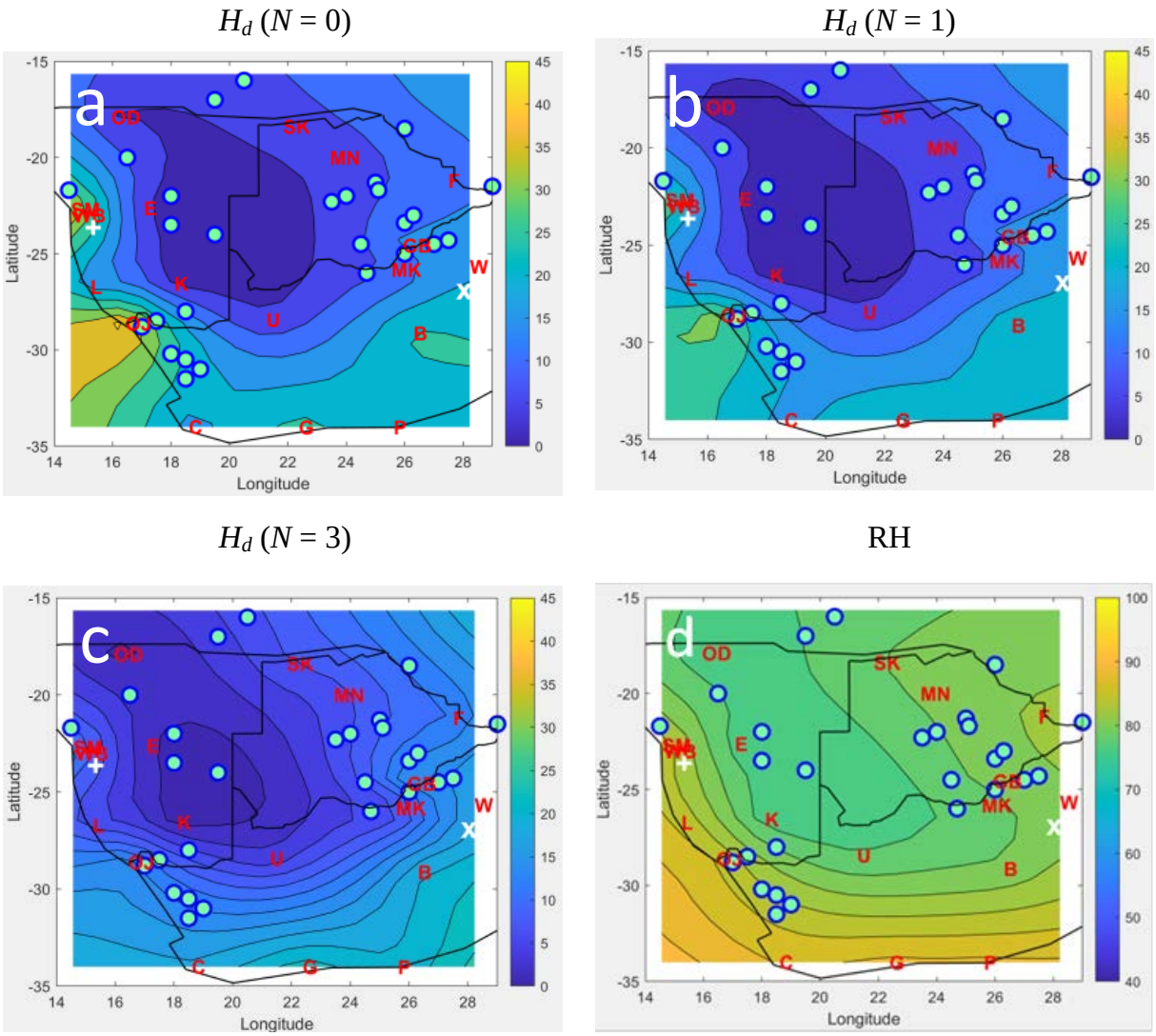

828

829 Fig. 2. (a, b, c): Map of annual dew yield H_d (in mm) in the period 2001 – 2020

830 corresponding to three scenarios for missing N data (see text and Table 1). (d): Mean

831 nocturnal RH (%) during dew events. Red letters: Meteo sites (see Table 1); circles: Biocrust

832 sites according to Chen et al., 2020; right cross: Gobabeb site studied by Henschel et al., 2007

833 and Soderberg, 2010; inclined cross: Potchefstroom site studied by Baier (1966).

834

835

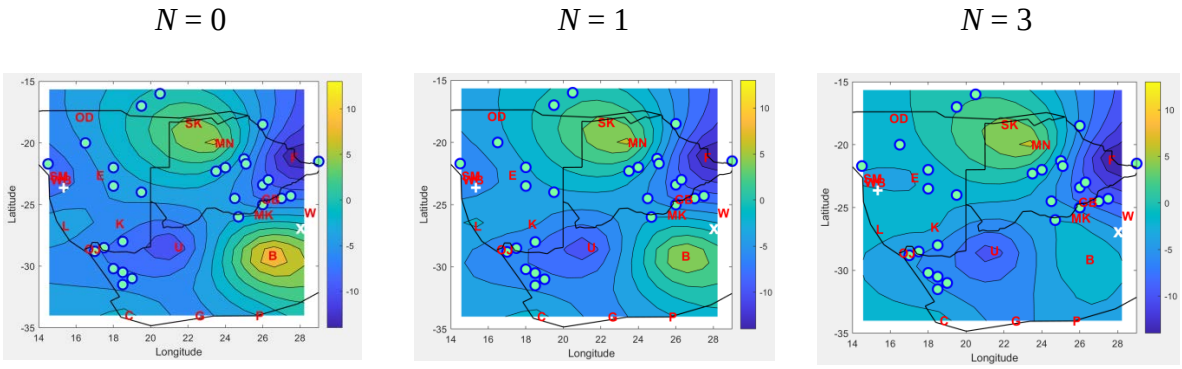

836 Fig. 3. Difference between 2020 and 2011 annual dew yields (mm) for three scenarios
837 corresponding to the missing *N* data (see text and Table 1). Red letters: Measurement sites
838 (see Table 1); circles: biocrust sites according to Chen et al., 2020; right cross: Gobabeb site
839 studied by Henschel et al., 2007 and Soderberg, 2010; inclined cross: Potchefstroom site
840 studied by Baier (1966).

841

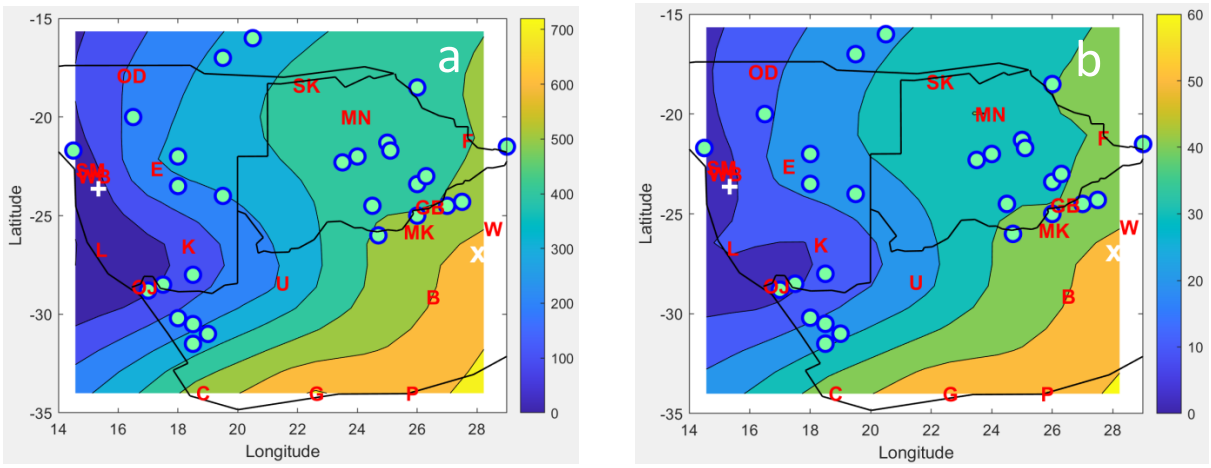

842

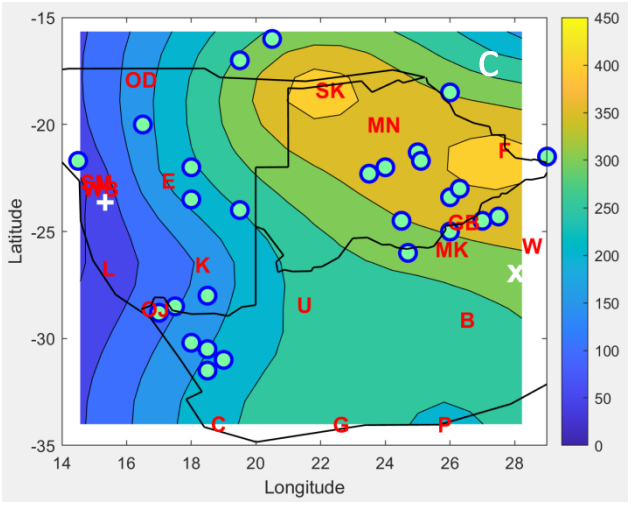

843 Fig. 4. Mean rainfalls (mm) during the period 2001 - 2020. (a) Mean annual rainfall. (b) Mean
844 monthly rainfall. (c) Maximum monthly rainfall. Red letters: Measurement sites (see Table 1);
845 circles: biocrust sites according to Chen et al., 2020; right cross: Gobabeb site studied by
846 Henschel et al., 2007 and Soderberg, 2010; inclined cross: Potchefstroom site studied by
847 Baier (1966).

848

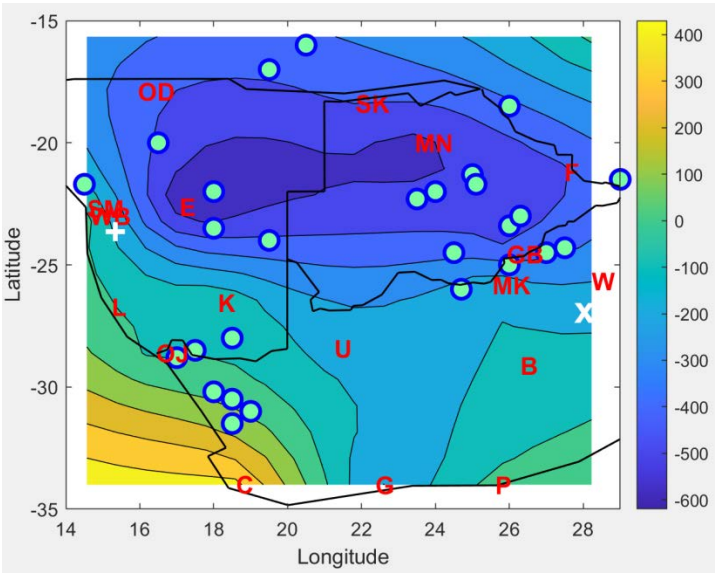

849

850 Fig. 5. Difference between 2020 and 2011 of the annual rainfalls (mm). Red letters:
851 Measurement sites (see Table 1); circles: biocrust sites from Chen et al., 2020; right cross:
852 Gobabeb site studied by Henschel et al., 2007 and Soderberg, 2010; inclined cross:
853 Potchefstroom site studied by Baier (1966).

854

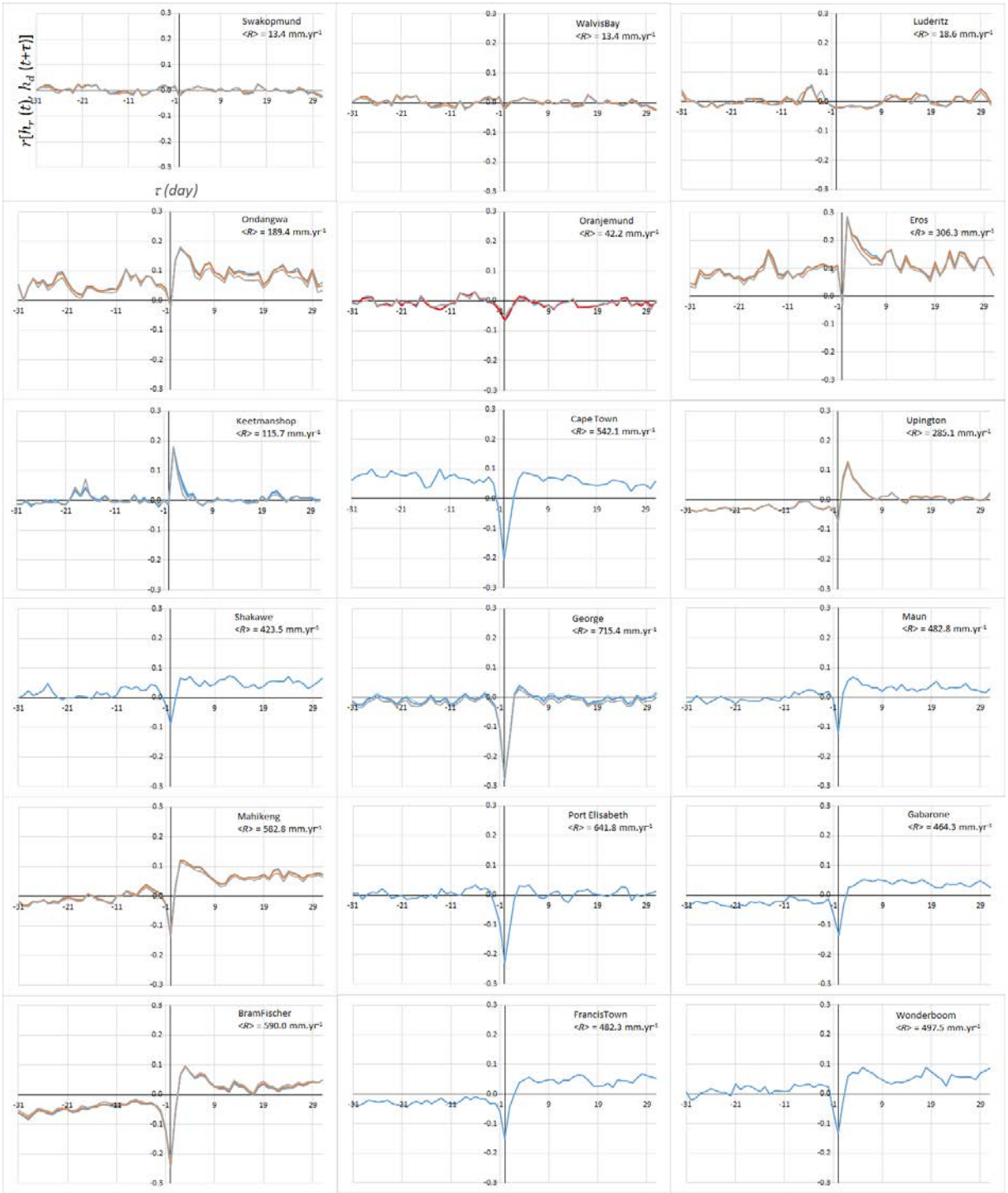

Fig. 6. Daily correlation coefficients $r[h_r(t), h_d(t+\tau)]$ for time $\tau \epsilon [-31 \; -+31]$ days. For stations with incomplete cloud cover data, the curves are presented assuming N = 0 (blue), N = 1 (red) and N = 3 (grey).

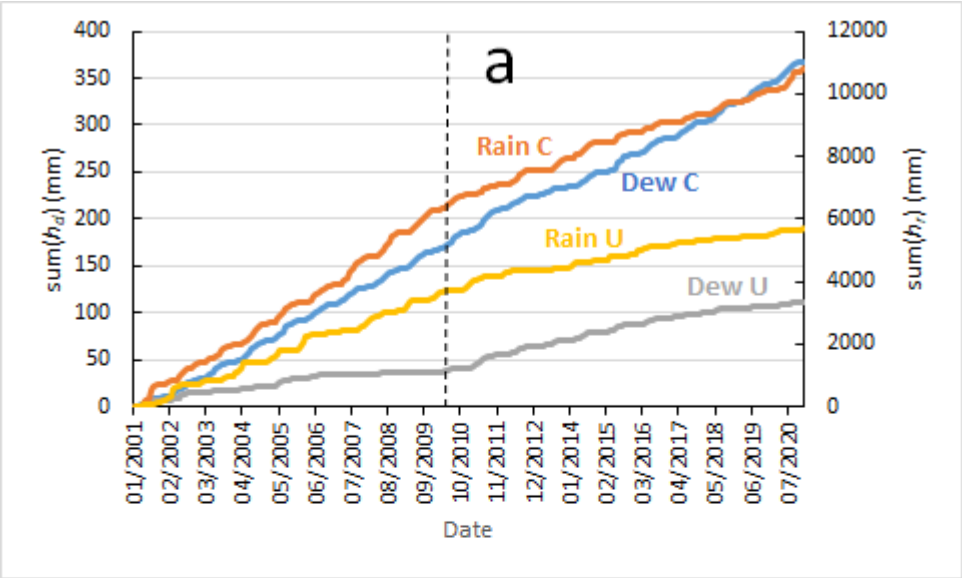

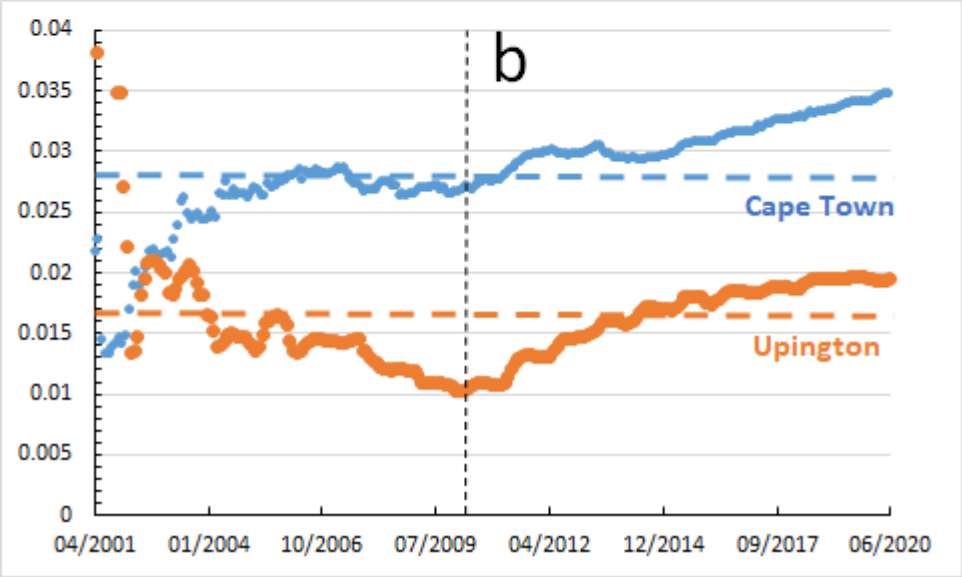

Fig. 7. Two typical evolutions (Upington and Cape Town sites) of dew and rain summed yields in the studied period (2001 – 2020). The vertical dotted line corresponds to year 2010 where rainfalls begin to significantly decrease. (a) $\mathrm{sum}(h_d)$ and $\mathrm{sum}(h_r)$ with N = 0 missing data scenario (see text and Table 1). (b) Ratio $a(t) = [\mathrm{sum}(h_d)]_t/[\mathrm{sum}(h_r)]_t$. The horizontal straight lines are fits to $a(t) = a_0$ = constant.

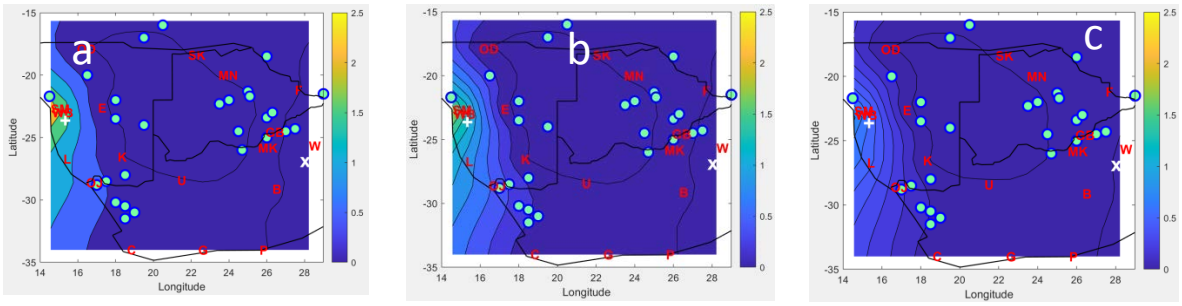

869 Fig. 8. Map of ratio a_0 corresponding to the average of a = sum(dew)/sum(rain) (Eqs. 8, 9) for
870 the period 2001 – 2020 and three scenarios for missing N data (see text and Table 1). Letters:
871 meteo sites; circles: biocrust sites according to Chen et al., 2020; right cross: Gobabeb site
872 studied by Henschel et al., 2007 and Soderberg, 2010; inclined cross: Potchefstroom site
873 studied by Baier (1966).

874

875

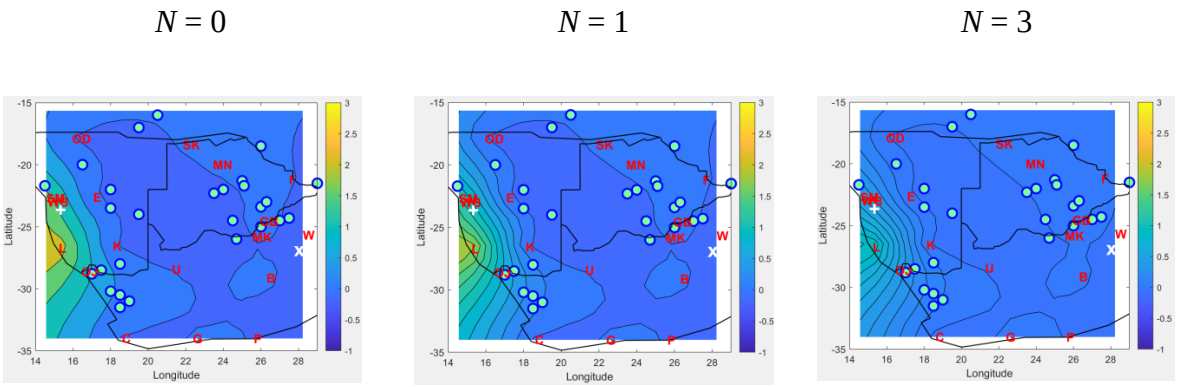

876

877 Fig. 9. Variation between 2020 and 2011 of the ratio *a* = sum(dew)/sum(rain), corresponding
878 to 3 scenarios for missing *N* data (see text and Table 1). Letters: meteo sites; circles: biocrust
879 sites according to Chen et al., 2020; right cross: Gobabeb site studied by Henschel et al., 2007
880 and Soderberg, 2010; inclined cross: Potchefstroom site studied by Baier (1966).

881

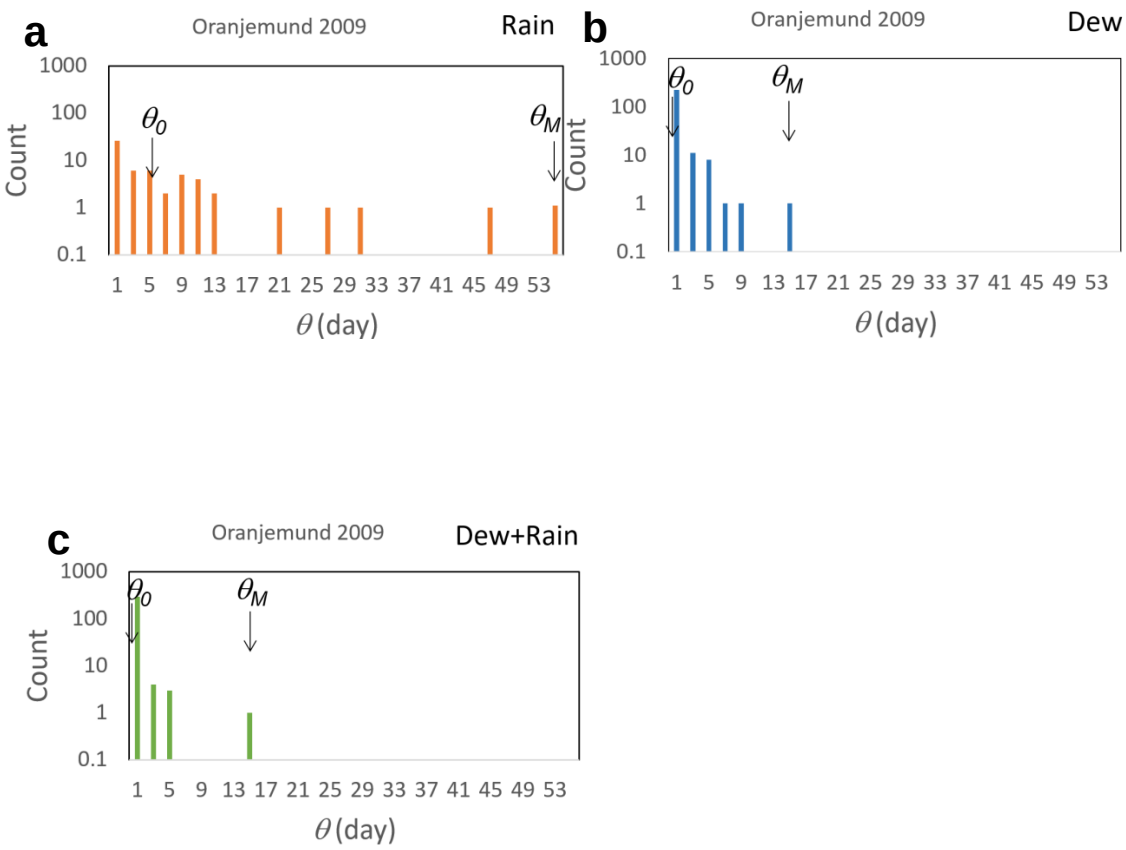

Fig. 10. Typical histograms of time period θ (day) beetween (a) rain events, (b) dew events (c) rain and dew events. θ_0 is the mean time and θ_M is the maximum time. Note that dew or rain events have diseppeared in the histogram dew + rain because dew or rain events occur during the dew or rain time periods.

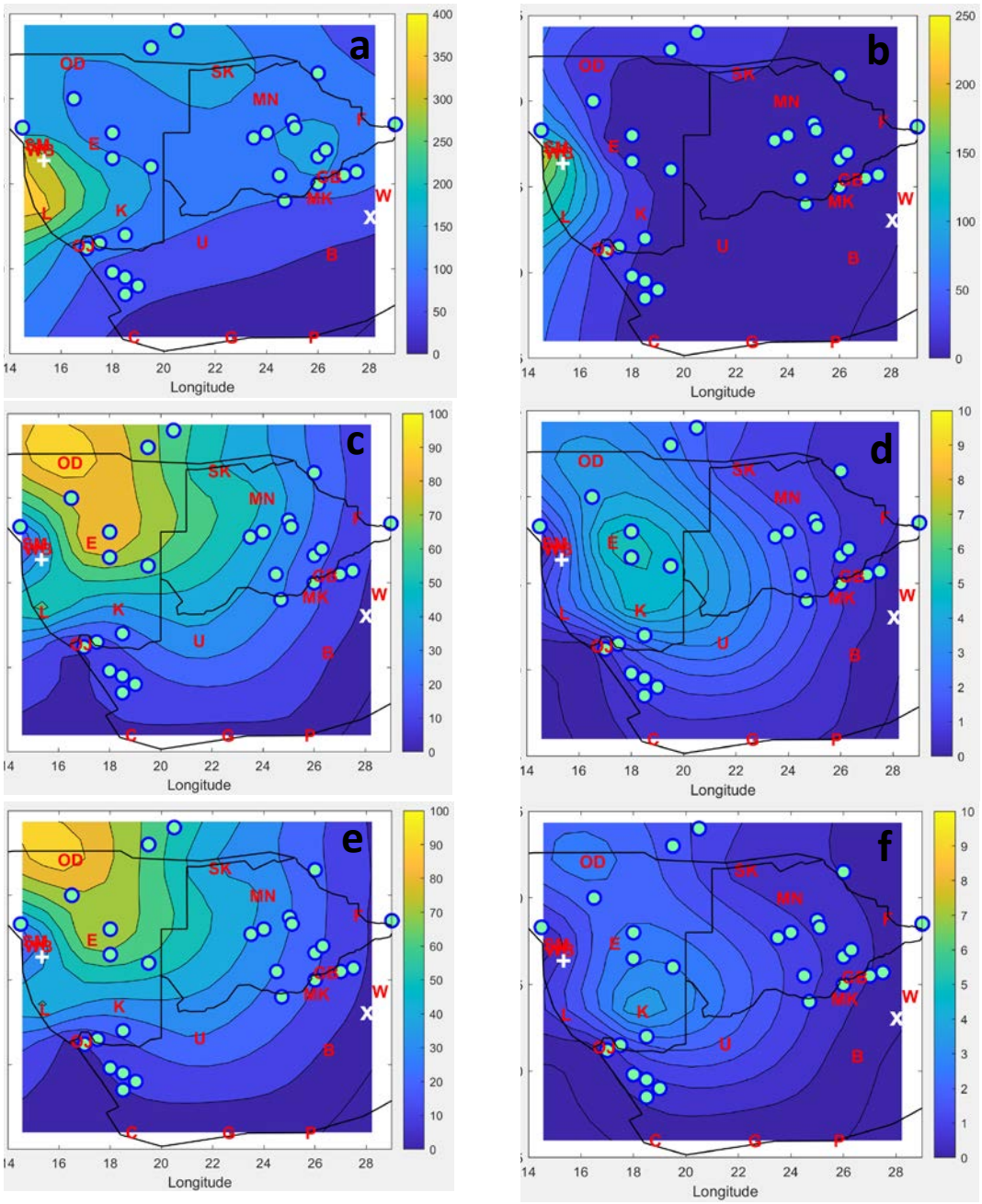

893

894

895 Fig. 11. Annual mean in the period 2001 – 2020 of the maximum time θ_M (day) (left column)
896 and mean time θ_0 (day) (right column). (a), (b): Rain; (c), (d): Dew; (e), (f): Rain+dew. Red
897 letters: Measurement sites (see Table 1); circles: biocrust sites according to Chen et al., 2020;

898 right cross: Gobabeb site studied by Henschel et al., 2007 and Soderberg, 2010; inclined
899 cross: Potchefstroom site studied by Baier (1966).

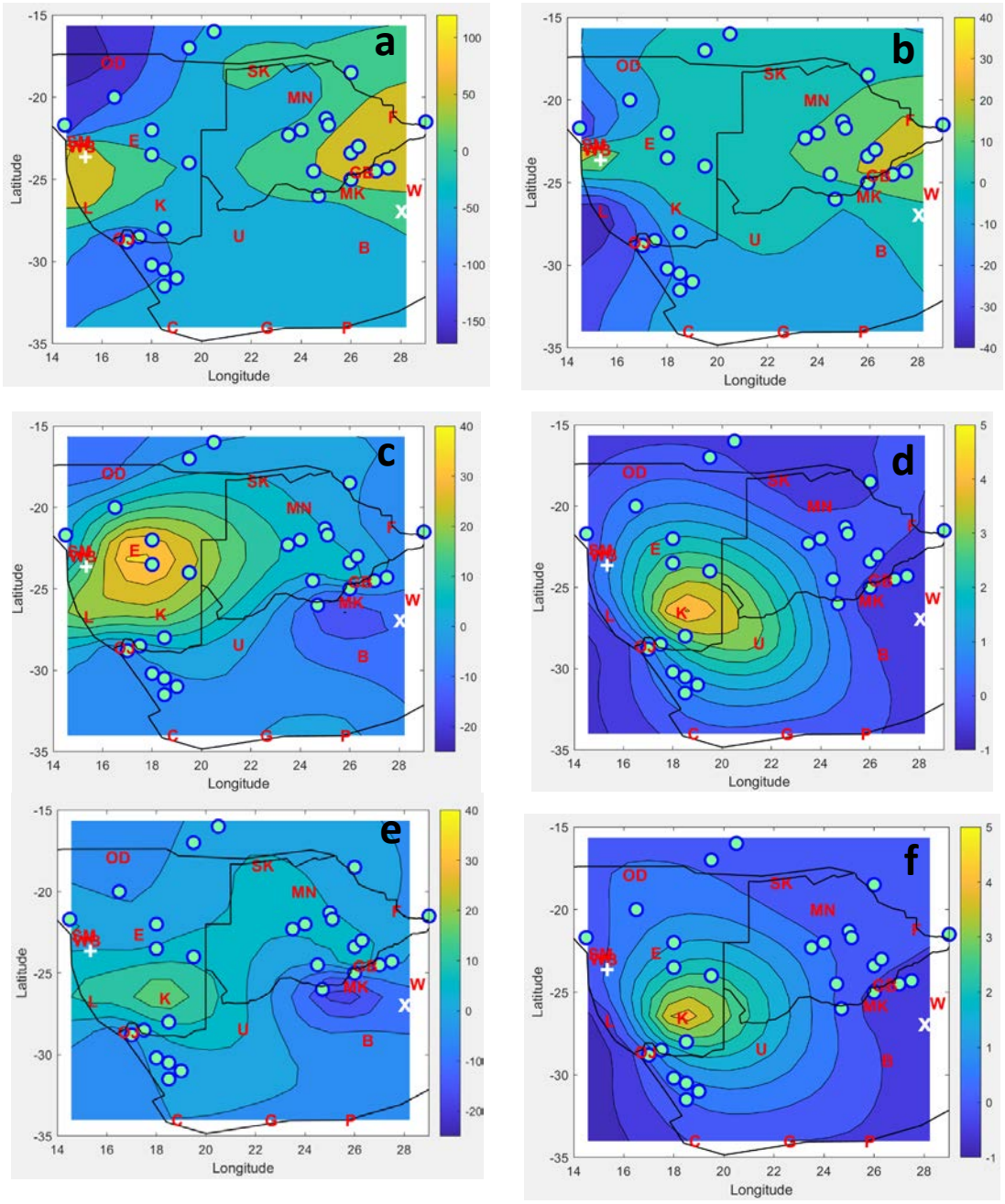

Fig. 12. Difference between 2020 and 2011 of the maximum time θ_M (left column, day) and mean time θ_0 (right column, day). (a), (b): Rain; (c), (d): Dew; (e), (f): Rain+dew. Red letters: Measurement sites (see Table 1); circles: biocrust sites from Chen et al., 2020; right cross: Gobabeb site studied by Henschel et al., 2007 and Soderberg, 2010; inclined cross: Potchefstroom site studied by Baier (1966).

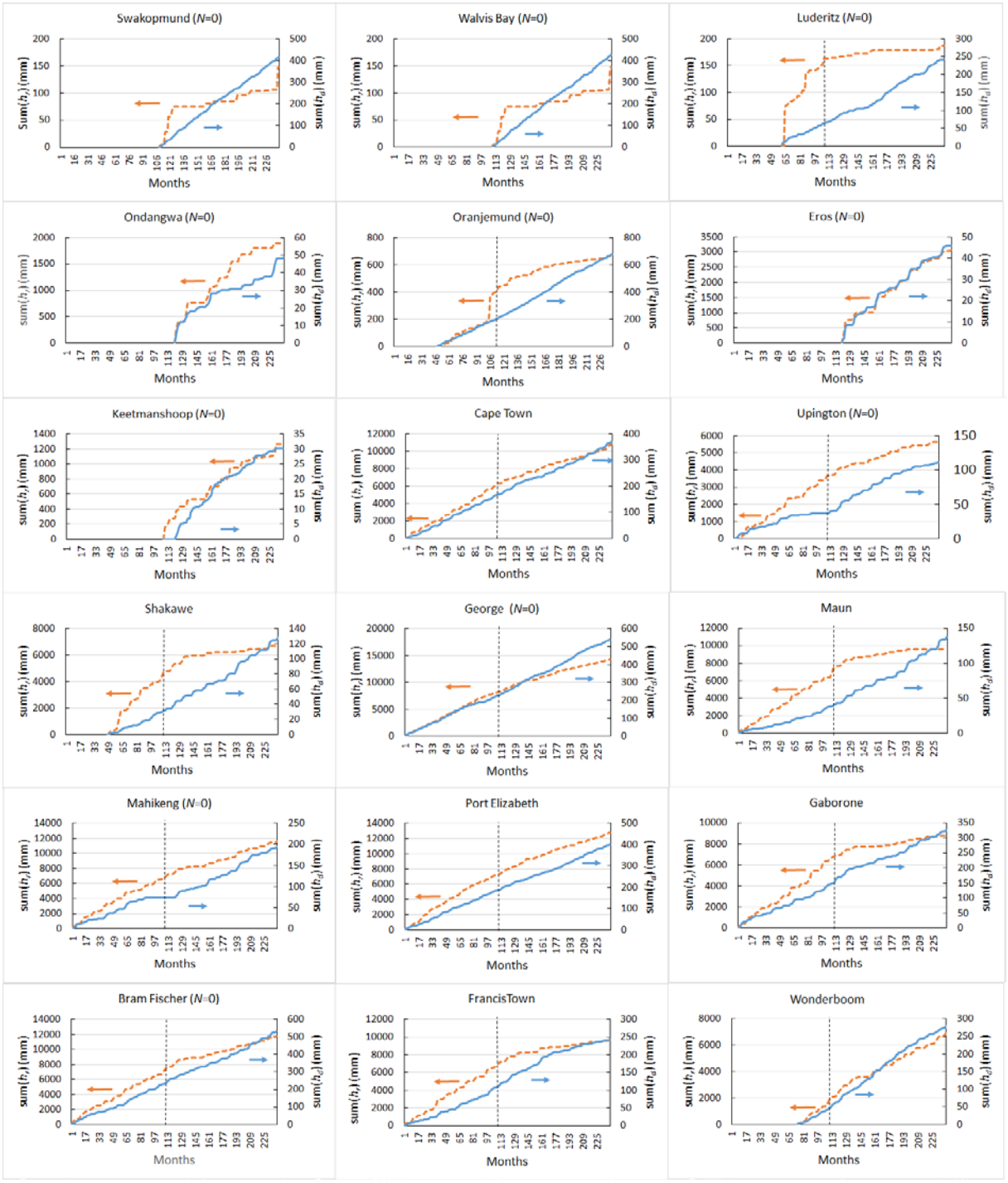

907

908 Fig. SM1. Evolution of the summed values sum(h_d) (dew, mm, full blue line) and sum(h_r)
909 (rain, mm, interrupted red line) for the studied sites. The vertical interrupted line corresponds
910 to a significant decrease of rainfall after 2010 with dew yield remaining constant or weakly
911 increasing.

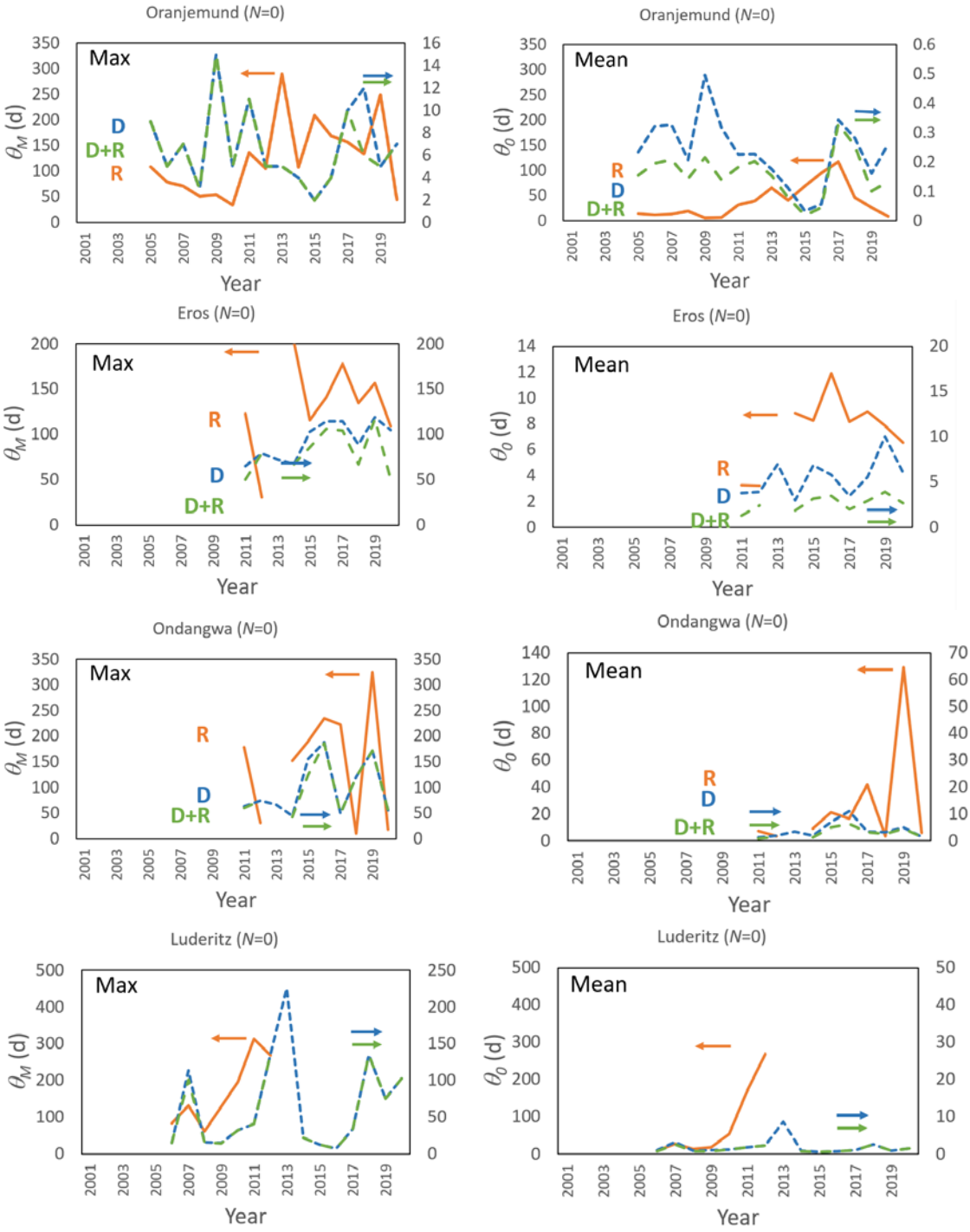
Oranjemund (N=0)
Max
D
D+R
R
θM (d)
Year
Oranjemund (N=0)
Mean
R
D
D+R
θ0 (d)
Year
Eros (N=0)
Max
R
D
D+R
θM (d)
Year
Eros (N=0)
Mean
R
D
D+R
θ0 (d)
Year
Ondangwa (N=0)
Max
R
D
D+R
θM (d)
Year
Ondangwa (N=0)
Mean
R
D
D+R
θ0 (d)
Year
Luderitz (N=0)
Max
θM (d)
Year
Luderitz (N=0)
Mean
θ0 (d)
Year

912

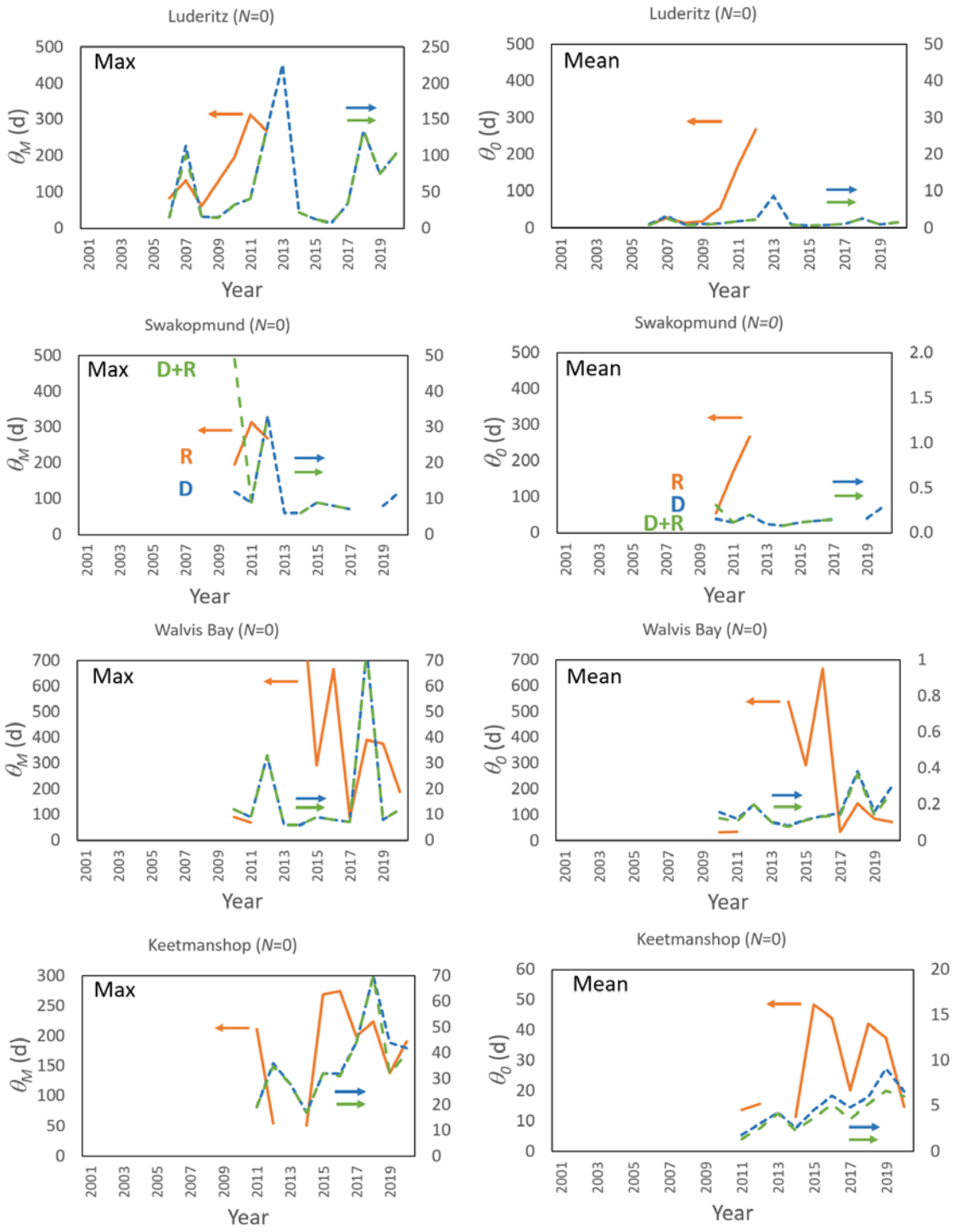
Luderitz (N=0)
Max
θM (d)
Year
Luderitz (N=0)
Mean
θ0 (d)
Year
Swakopmund (N=0)
Max
D+R
R
D
θM (d)
Year
Swakopmund (N=0)
Mean
R
D
D+R
θ0 (d)
Year
Walvis Bay (N=0)
Max
θM (d)
Year
Walvis Bay (N=0)
Mean
θ0 (d)
Year
Keetmanshop (N=0)
Max
θM (d)
Year
Keetmanshop (N=0)
Mean
θ0 (d)
Year

913

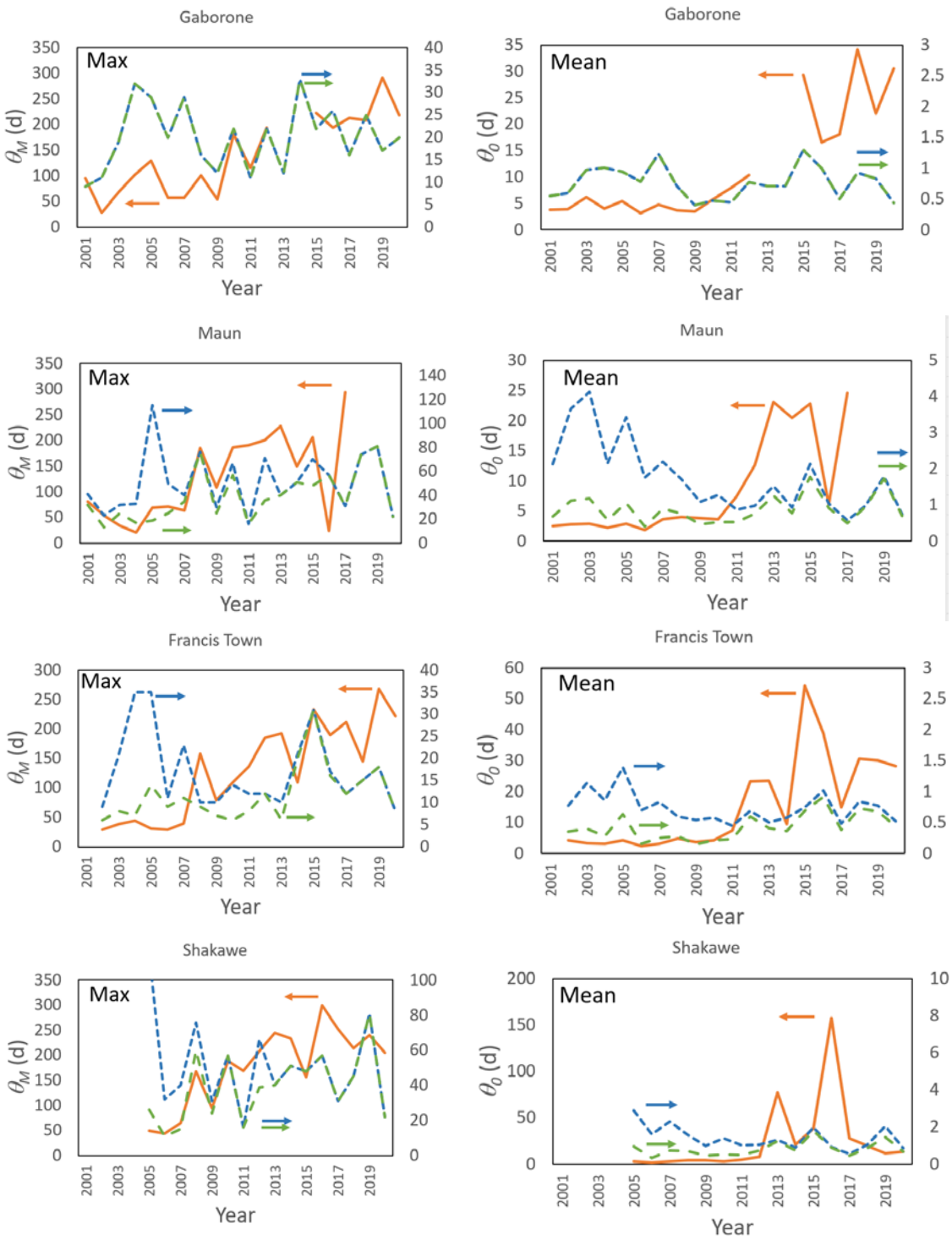
Gaborone
Max
θ_M (d)
Year
Gaborone
Mean
θ_0 (d)
Year
Maun
Max
θ_M (d)
Year
Maun
Mean
θ_0 (d)
Year
Francis Town
Max
θ_M (d)
Year
Francis Town
Mean
θ_0 (d)
Year
Shakawe
Max
θ_M (d)
Year
Shakawe
Mean
θ_0 (d)
Year

914

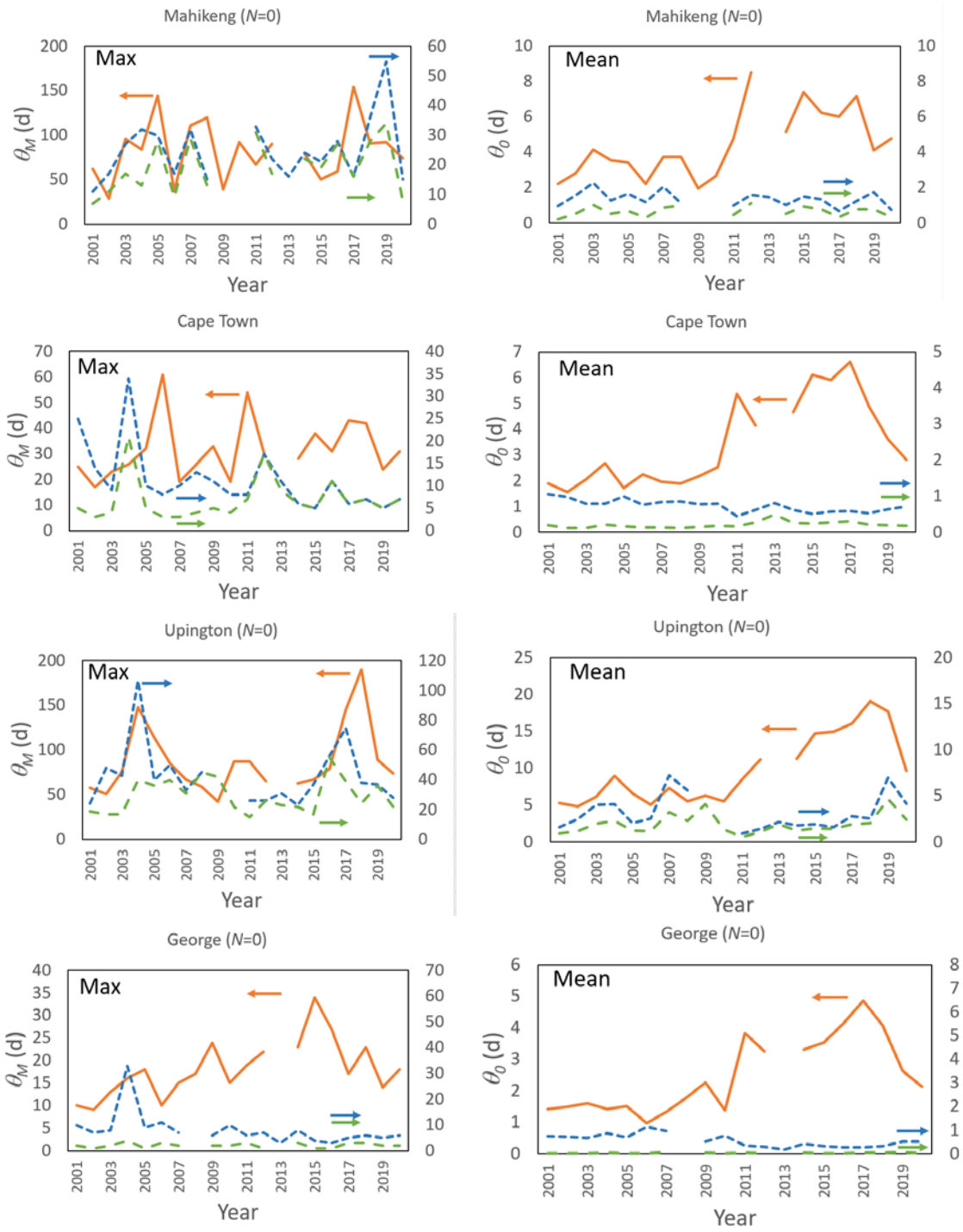
Mahikeng (N=0)
Max
Mean
Cape Town
Upington (N=0)
George (N=0)
θ_M (d)
θ_0 (d)
Year

915

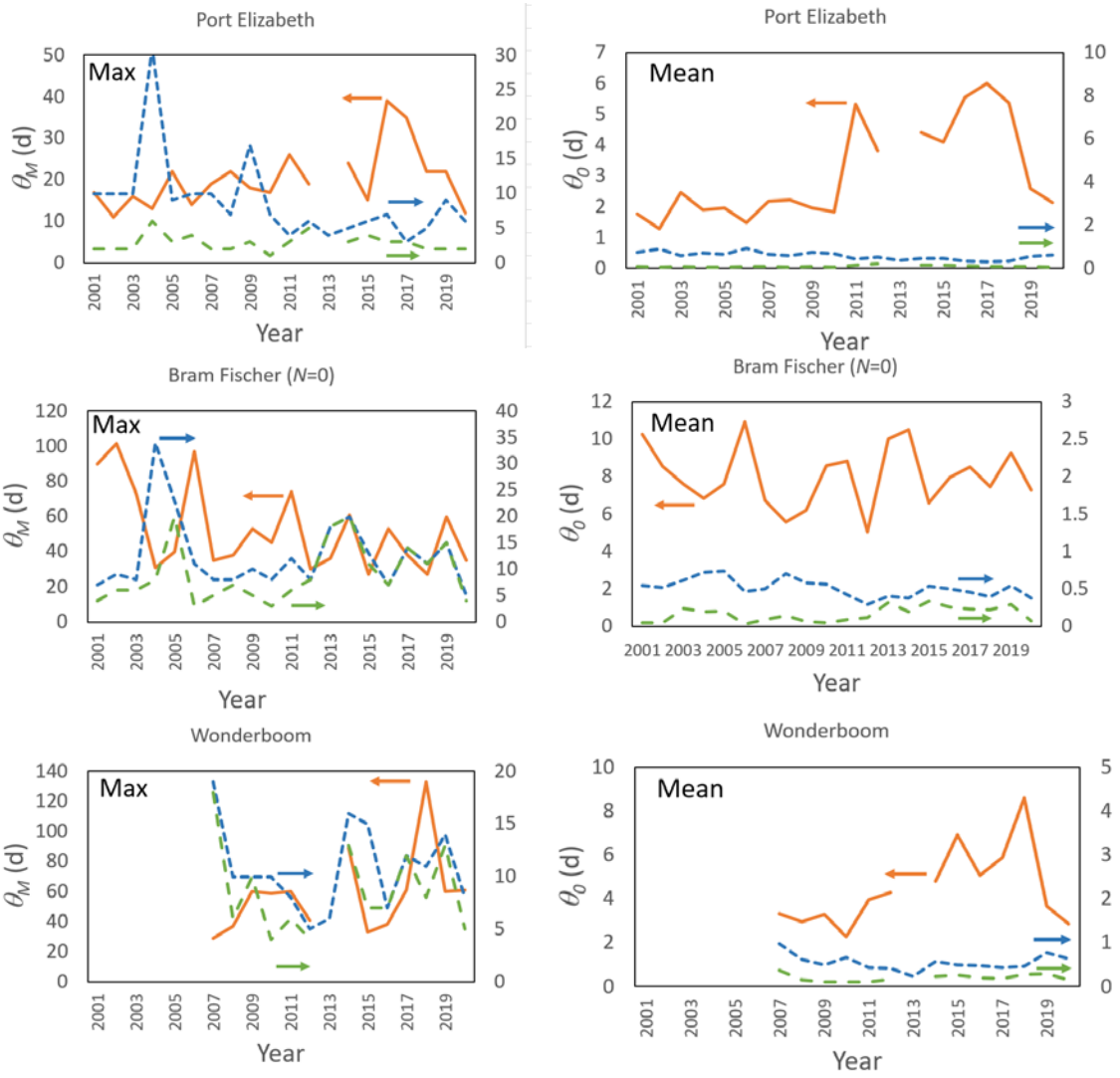

916

917 Fig. SM2. Evolution of mean time θ_0 (day) and maximum time θ_M (day) between (a) rain
918 (orange line), dew (blue short interrupted line) and rain plus dew events (green long
919 interrupted line). Some curves are interrupted because data are missing.

920

921

Country Name	Site	Abbreviations	Latitude	Longitude	Altitude (m asl)	Distance to the sea (km)	data period	Sky conditions data (%)
Namibia	Swakopmund	SM	22° 40' 0'' S	14° 34' 0'' E	61	8	2010-2020	52.4
Namibia	Walvis Bay	WB	22° 58′ 47″ S	14° 38′ 43″ E	86	14	2010-2020	52.4
Namibia	Luderitz	L	26° 41′ 15″ S	15° 14′ 34″ E	131	1	2006-2020	0.0
Namibia	Ondangwa	OD	17° 52′ 41″ S	15° 57′ 09″ E	1099	385	2011-2020	47.7
Namibia	Oranjemund	OJ	28° 35′ 05″ S	16° 26′ 48″ E	5	6	2005-2020	0.0
Namibia	Eros	E	22° 36′ 44″ S	17° 04′ 50″ E	1699	266	2011-2020	45.2
Namibia	Keetmanshoop	K	26° 32' 13'' S	18° 06′ 40″ E	1069	285	2011-2020	40.0
South Africa	Cape Town	C	33° 58′ 10″ S	18° 35′ 50″ E	46	3	2001-2020	100.0
South Africa	Upington	U	28° 24′ 04″ S	21° 15′ 35″ E	844	432	2001-2020	77.3
Botswana	Shakawe	SK	18° 22′ 25″ S	21°50′ 00″ E	1008	895	2005-2020	100.0
South Africa	George	G	34° 0' 20'' S	22° 22' 42'' E	197	7	2001-2020	89.9
Botswana	Maun	MN	19° 59' 0'' S	23° 26' 0'' E	945	1106	2001-2020	100.0
South Africa	Mahikeng	MK	25° 48' 27"S	25° 32' 40" E	1274	680	2001-2020	65.6
South Africa	Port Elizabeth	P	33° 59' 5'' S	25° 37' 2'' E	68	3	2001-2020	100.0
Botswana	Gaborone	GB	24° 33′ 19″ S	25° 55′ 06″ E	1006	695	2001-2020	99.9
South Africa	Bram Fischer	B	29° 05′ 38″ S	26° 18′ 14″ E	1349	418	2001-2020	76.1
Botswana	Francistown	F	21° 10' 0'' S	27° 29' 0'' E	1002	726	2002-2020	100.0
South Africa	Wonderboom	W	25° 39′ 13″ S	28° 13′ 27″ E	1240	460	2005-2020	88.6

Table 1. Sites where atmospheric data are collected (7 stations in Namibia, 4 stations in Bostwana and 7 stations in South Africa). They are sorted according to their longitude (west to east). The sky condition data availability (% of the total sky conditions data) is reported for each station.

930

Site	H_r (mm.yr^{-1})			h_r (mm)			α_r (mm.month^{-1})	$h_{r,0}$ (mm)	yearly frequency (%)
	Mean	Min	Max	Mean	Min	Max			
Swakopmund	**13.4**	0.0	56.0	**1.1**	0.0	41.2	-0.005	1.5	0.9
Walvis Bay	**13.4**	0.0	56.0	**1.1**	0.0	41.2	-0.005	1.5	0.9
Luderitz	**18.6**	1.0	83.5	**12.4**	0.0	64.1	-0.024	3.2	1.8
Ondangwa	**189.4**	6.6	453.0	**15.8**	0.0	155.0	-0.283	32.9	5.3
Oranjemund	**42.2**	7.0	225.8	**3.5**	0.0	115.6	-0.030	6.4	5.0
Eros	**306.3**	115.2	824.0	**25.5**	0.0	204.0	-0.275	42.2	10.9
Keetmanshoop	**115.7**	20.8	278.4	**9.6**	0.0	145.1	-0.044	11.0	3.7
Cape Town	**542.1**	249.0	888.8	**45.2**	0.0	238.0	-0.148	57.0	24.8
Upington	**285.1**	53.0	518.4	**23.8**	0.0	261.4	-0.167	38.3	10.4

Shakawe	**423.5**	8.4	1072.3	**35.3**	0.0	447.1	-0.493	82.8	13.0
George	**715.4**	333.0	1223.7	**59.6**	0.0	290.5	-0.260	79.7	30.7
Maun	**482.8**	20.0	1115.9	**40.2**	0.0	375.3	-0.468	79.8	14.9
Mahikeng	**582.8**	182.0	1158.1	**48.6**	0.0	320.3	-0.135	55.5	19.7
Port Elizabeth	**641.8**	308.0	1103.8	**53.5**	0.0	235.5	-0.171	64.2	26.8
Gaborone	**464.3**	80.2	1023.3	**38.7**	0.0	372.5	-0.374	68.0	11.9
Bram Fischer	**590.0**	160.0	1190.0	**49.2**	0.0	274.7	-0.253	68.8	20.2
Francistown	**482.3**	46.2	1199.9	**40.2**	0.0	423.3	-0.342	66.2	13.6
Wonderboom	**497.5**	123.0	769.9	**41.5**	0.0	183.6	-0.095	49.9	18.5

931

932 Table 2. Mean, minimum and maximum yearly (H_r) and monthly (h_r) rainfall calculated from
933 meteorological from 2001 to 2020 are fitted to Eq. 5 with free parameters $\alpha_r = dh_r/dt$ and
934 $h_{r,0}$.

Site	a (N=0)	a (N=1)	a (N=3)
Swakopmund	2.384	1.793	0.792
Walvis Bay	2.444	1.841	0.832
Luderitz	1.154	0.940	0.569
Ondangwa	0.023	0.016	0.006
Oranjemund	0.858	0.651	0.282
Eros	0.014	0.011	0.006
Keetmanshoop	0.020	0.014	0.006
Cape Town	0.028	0.028	0.028
Upington	0.017	0.015	0.012
Shakawe	0.011	0.011	0.011
George	0.031	0.027	0.024
Maun	0.007	0.007	0.007
Mahikeng	0.013	0.011	0.007
Port Elizabeth	0.026	0.026	0.026
Gaborone	0.028	0.028	0.028
Bram Fischer	0.034	0.032	0.029
Francistown	0.018	0.018	0.018
Wonderboom	0.034	0.034	0.034

935

936 Table 3. Ratio dew/rain summed amplitudes a_0 (Eq. 9) according to different N assumptions
937 for the missing data (see text and Table 1).

938

Observation	*N* (oktas)
CLR	0
FEW	1
SCT	3
BKN	5
OVC	8

Table SM1. Correlation between sky conditions and cloud cover according to NOAA, 2021. The abbreviations for sky conditions are the following: CLR = Clear; FEW = few; SCT = Scattered; BKN = Broken; OVC = Overcast.

944

Site	N (oktas)	H_d (mm)			h_d (mm)			α_d (mm.month^{-1})	$h_{d,0}$ (mm)	yearly frequency (%)
		Mean	Min	Max	Mean	Min	Max			
Swakopmund	0	**37.7**	31.2	45.5	**3.1**	0.0	6.8	-0.002	3.2	85.6
	1	**28.4**	22.9	34.6	**2.4**	0.0	5.4	-0.001	2.4	84.9
	3	**12.6**	9.4	15.9	**1.0**	0.0	2.8	-0.001	1.1	79.1
Walvis Bay	0	**38.2**	31.7	46.1	**3.2**	0.0	6.9	-0.002	3.2	85.8
	1	**28.8**	23.3	35.1	**2.4**	0.0	5.4	-0.001	2.4	85.0
	3	**12.8**	9.6	16.1	**1.0**	0.0	2.9	-0.001	1.1	79.3
Luderitz	0	**16.2**	3.6	26.3	**1.3**	0.0	4.9	0.001	1.3	42.3
	1	**12.6**	2.8	21.4	**1.0**	0.0	4.3	0.001	0.1	40.3
	3	**6.6**	1.3	13.3	**0.6**	0.0	3.0	0.000	0.5	34.8
Ondangwa	0	**4.9**	0.4	13.5	**0.4**	0.0	3.7	-0.004	0.6	25.3
	1	**3.5**	0.3	9.8	**0.3**	0.0	2.8	-0.003	0.5	22.0
	3	**1.4**	0.1	3.8	**0.1**	0.0	1.2	-0.001	0.2	13.5
Oranjemund	0	**42.5**	32.4	56.8	**3.5**	0.9	8.2	0.003	3.2	81.5
	1	**32.8**	23.9	45.2	**2.7**	0.5	6.8	0.003	2.4	80.4
	3	**15.4**	9.6	24.3	**1.3**	0.2	4.1	0.003	1.0	70.6
Eros	0	**4.6**	1.4	8.9	**0.4**	0.0	2.6	-0.004	0.6	16.7
	1	**3.5**	0.9	7.0	**0.3**	0.0	2.1	-0.003	0.5	14.6
	3	**1.9**	0.3	3.8	**0.2**	0.0	1.1	-0.002	0.3	13.3
Keetmanshoop	0	**3.0**	0.8	5.7	**0.3**	0.0	1.8	-0.003	0.5	18.4
	1	**2.2**	0.5	4.2	**0.2**	0.0	1.4	-0.002	0.3	15.3
	3	**0.9**	0.2	2.0	**0.1**	0.0	0.8	-0.001	0.1	8.7
Cape Town	-	**18.3**	8.9	24.1	**1.5**	0.0	5.1	0.000	1.6	58.2

Upington	0	**5.5**	0.4	13.8	**0.5**	0.0	2.9	0.000	0.5	27.0
	1	**5.1**	0.4	13.2	**0.4**	0.0	2.8	0.000	0.4	26.6
	3	**4.5**	0.4	12.4	**0.4**	0.0	2.6	0.001	0.3	25.7
Shakawe	-	**8.0**	3.5	16.5	**0.7**	0.0	4.5	0.003	0.4	43.9
George	0	**27.0**	12.8	38.5	**2.2**	0.0	4.7	0.004	2.1	64.5
	1	**25.7**	12.8	37.4	**2.1**	0.0	4.7	0.003	1.9	64.3
	3	**23.3**	12.8	35.3	**1.9**	0.0	4.7	0.002	1.6	64.0
Maun	-	**6.9**	1.8	18.0	**0.6**	0.0	4.9	0.003	0.3	40.3
Mahikeng	0	**9.8**	0.1	21.7	**0.8**	0.0	4.7	0.003	0.6	37.6
	1	**8.1**	0.1	18.1	**0.7**	0.0	4.1	0.002	0.5	35.8
	3	**5.5**	0.1	12.2	**0.5**	0.0	2.9	0.001	0.3	33.2
Port Elizabeth	-	**20.0**	14.3	26.8	**1.7**	0.0	4.5	0.000	1.6	64.1
Gaborone	-	**16.2**	6.6	26.0	**1.4**	0.0	5.9	-0.001	1.4	57.8
Bram Fischer	0	**26.5**	14.4	38.8	**2.2**	0.0	7.7	0.001	2.2	66.4
	1	**24.0**	11.9	38.7	**2.0**	0.0	6.8	0.000	2.2	65.6
	3	**20.1**	8.7	38.4	**1.7**	0.0	5.6	0.000	2.2	64.8
Francistown	-	**12.1**	4.9	23.8	**1.0**	0.0	4.2	-0.004	1.4	58.3
Wonderboom	-	**19.9**	8.0	27.4	**1.7**	0.0	5.0	0.000	1.7	65.5

Table SM2. Yearly (H_d) and monthly (h_d) mean, minimum and maximum dew yields calculated from meteorological data. The mean evolution data during from 2001 to 2020 are fitted to Eq. 5 with free parameters $\alpha_d = dh_d/dt$ and $h_{d,0}$. Red values correspond to a decrease of dew yield evolution, blue values to an increase. Cloud coverage N is assumed to be 0, 1 or 3 oktas when cloud cover data are missing (see text and Table 1).